R. & M. No. 3570

MINISTRY OF TECHNOLOGY

AERONAUTICAL RESEARCH COUNCIL
REPORTS AND MEMORANDA

An Experimental Investigation of Wall-Interference Effects on Dynamic Measurements on Half-Models in Ventilated Tunnels through the Transonic Speed Range

By A. W. Moore and K. C. Wight

LONDON: HER MAJESTY'S STATIONERY OFFICE
1969
PRICE £1 3*s.* 0*d.* NET

An Experimental Investigation of Wall-Interference Effects on Dynamic Measurements on Half-Models in Ventilated Tunnels through the Transonic Speed Range

By A. W. Moore and K. C. Wight

Reports and Memoranda No. 3570*
August, 1967

Summary.

Results are presented of an experimental investigation of ventilated-wall interference on dynamic measurements using half-models in four transonic tunnels, three of which have a slotted roof and floor whilst the other has a perforated roof and floor. It is shown that if wall interference effects are present at subsonic speeds then these probably persist to low supersonic speeds. The supersonic interference can be associated with an upstream propagation of disturbances in the plenum chambers in a region close to the ventilated walls.

The interference effects in the perforated tunnel are comparable with those produced previously when it was fitted with a slotted roof and floor. It is found that variation of diffuser suction to the plenum chambers behind the perforated walls has a significant effect on the damping derivatives.

With the half-model technique used, both lift and pitching-moment derivatives are shown to be influenced by the thickness of the side-wall boundary layer, but in many practical cases the effect may be acceptably small.

CONTENTS

Section.

*Replaces N.P.L. Aero. Report 1243—A.R.C. 29 331.

LIST OF TABLES

1. *Introduction.*

In order to achieve a flow whose speed may be varied continuously from subsonic to supersonic, it is necessary to use wind tunnels with ventilated walls. The ventilations may consist of longitudinal slots or circular perforations in the whole tunnel boundary, but in many tunnels only the roof and floor are ventilated. Extensive investigation of the effects of ventilated walls in steady flow has produced well established criteria by which lift and blockage interference may be minimised and the resulting small corrections to measured results calculated; *see* Refs. 1 and 2 for instance.

Serious doubts[3] were raised as to the value of dynamic measurements made in some tunnels with slotted roof and floor when large changes in pitching damping of half-wing models were produced by progressively sealing the slots. A theoretical explanation of this phenomenon has only recently been found[4]. With the simplifying assumptions of a small wing and a low frequency of oscillation, the lift interference effects at subsonic speeds can be satisfactorily predicted when the ventilated walls operate near to the limiting condition of an open boundary. For slotted walls which are not subject to significant viscous effects, an allowance can be made for slot geometry. The theoretical work was combined with a parallel experimental investigation using wall-mounted half-models in slotted tunnels. In general, good agreement in magnitude and trend between the measured and predicted interference was obtained. An approximate method for correcting measured derivatives to free-stream conditions was formulated. For small half-models tested in the larger tunnels, the corrected results were significantly displaced from the expected interference-free values, and this was attributed to effects of the tunnel side-wall boundary layer.

The primary object of the present work is to extend the experimental investigation into the transonic speed range. It is apparent from Ref. 4 that the subsonic interference effects increase with Mach number in the range $0 \leqslant M \leqslant 0{\cdot}85$. This suggests that large effects might occur in the transonic speed range where the theory would not be expected to apply. Measurements have therefore been made on a half-delta model in four transonic tunnels, three with slotted roof and floor and one with a perforated roof and floor. At the same time, the opportunity arose to extend the previous subsonic investigation by examining the effect of the different side-wall boundary layers on the same model. These results are discussed in Section 4.1. It is also shown that, at subsonic speeds, perforated walls can produce interference effects on damping derivatives just as large as those due to slotted walls. This had been expected on theoretical grounds for walls with high porosity but no previous experimental evidence was available. An important corollary to these measurements is the discovery of large changes in the value of the damping derivative due to changes in the diffuser suction applied to the plenum chamber. In Section 4.2 it is shown that if large interference effects are present at subsonic speeds, then they persist up to low supersonic speeds. Indeed, in Section 4.3 there is evidence from the measured lift damping on a symmetrically tapered wing in a perforated tunnel to show that a form of ventilated wall interference (apart from Mach wave reflection) exists at Mach numbers up to $M = 1{\cdot}35$ at least.

The subsonic interference is associated with wall constraint on the upwash propagated upstream to the oscillating model. Although there can be no upstream propagation in a supersonic flow, results discussed in Section 4.2 show that induced upwash is present at the model throughout the transonic speed range. Furthermore, an induced upwash in the main stream ahead of a model oscillating in a slotted tunnel has recently been measured[5] at a supersonic Mach number $M = 1{\cdot}14$. Such upwash appears to be induced *via* the plenum chamber, but in view of the apparent similarity of the measured interference effects at subsonic and transonic speeds, the method of correction for subsonic speeds is tentatively applied to the present measurements up to $M = 1{\cdot}1$ and plausible corrections appear to be produced.

2. *Method and Scope of Measurements.*

Tests using the two half-models shown in Fig. 1 have been made in four transonic tunnels. Each model has a roughness band near the leading edge to fix boundary-layer transition. Cross-sections of the four tunnels used are shown in Fig. 2 and further details are given in Table 2. It might be noted that all the tunnels have solid side-walls and that three have only a slotted roof and floor whilst the 25 in. × 20 in. Tunnel has, in addition, alternative perforated liners. These perforated liners are flexible so that moderately high supersonic Mach numbers can be achieved. The half-delta model with aspect ratio 2·64 was tested at speeds in the range $0{\cdot}4 \leqslant M \leqslant 1{\cdot}1$ in all of the tunnels. The ratios of model area to tunnel cross-sectional area obtained were in the range $0{\cdot}02 < S/C < 0{\cdot}14$. Pitching-moment derivatives were measured using the rig described in Ref. 4. In essence, the method is to release the model from a displaced position, to record electronically, and then to analyse the resulting decaying oscillations. The pitching damping derivative $m_{\dot{\theta}}$ is determined from successive measurements with 'wind-on' and in 'still air', whilst the pitching stiffness derivative m_θ is calculated from the corresponding change in the frequency of the decaying oscillations. Derivatives have been measured in this way about three pitching axes ($x_0 = 0{\cdot}31\bar{c}, x_0 = 0{\cdot}65\bar{c}$, $x_0 = 1{\cdot}04\bar{c}$) using the same nominal frequency of oscillation of 53 *Hz*.

Further to these results, the half-model of symmetrically tapered planform with aspect ratio 4·33 has been tested in the perforated tunnel. Both pitching moment and lift derivatives were measured using the self-excited oscillation technique described in Ref. 6. Three pitching axis positions were used ($x_0 = 0{\cdot}395\bar{c}$, $x_0 = 0{\cdot}790\bar{c}$, $x_0 = 1{\cdot}185\bar{c}$) but lift could only be measured at the centre axis. With use of the flexible perforated walls, tests were done in the extended speed range $0{\cdot}4 \leqslant M \leqslant 1{\cdot}4$. The nominal frequency of oscillation for this model was 22 *Hz*.

3. *Presentation of Results.*

When the experiments with the delta wing were planned, it was decided to keep the rig as simple as possible so that it could easily be transported from one tunnel to another. A decaying oscillation technique in which only pitching-moment derivatives could be measured was therefore adopted. Knowledge of the lift damping derivative is particularly useful in this investigation because it is the derivative most sensitive to ventilated-wall interference[4]. Since pitching moment derivatives were usually measured about three pitching axes, values of the lift derivatives can be estimated using the following formulae:

$$l_{\theta 1} = l_{\theta 2} = \frac{m_{\theta 2} - m_{\theta 1}}{(x_2 - x_1)/\bar{c}} \tag{1}$$

$$l_{\dot{\theta} 1} - m_{\theta 2} = \frac{m_{\dot{\theta} 2} - m_{\dot{\theta} 1}}{(x_2 - x_1)/\bar{c}} = l_{\dot{\theta} 2} - m_{\theta 1} \tag{2}$$

where the equations are derived from the axis transfer relations on the assumption that, for low frequency parameters,

$$l_z = m_z = 0$$

$$l_{\dot{z}} = l_\theta$$

$$m_{\dot{z}} = m_\theta$$

and subscripts 1, 2 refer to pitching axes at distances x_1, x_2 downstream of the root chord leading edge, $\bar{c}$ being the mean chord of the model. All the lift derivatives presented for the delta-wing have been calculated from measurements at the most forward and the most rearward axis positions available. The tests with the symmetrically tapered wing in the perforated tunnel provided a means of checking these relations for a larger model. In this case a self-excited oscillation technique was used and lift as well as pitching-moment derivatives were measured at one axis position whilst pitching-moment derivatives

were measured at two other axis positions. Figs. 3a and 3b show comparisons between lift derivatives estimated from the measured pitching moment about axes $x_0 = 0{\cdot}395\bar{c}$, $x_0 = 1{\cdot}185\bar{c}$ and the lift derivatives measured directly. Even with this relatively large model, agreement is reasonably good, the only significant discrepancy occurring for the lift damping derivative around $M = 1{\cdot}1$ where its value is changing rapidly with Mach number. Other results obtained some years ago with the same model in the 36 in. × 14 in. Tunnel have been treated in the same way and there is again satisfactory agreement. Further use of the axis transfer relations is made in the consideration of the delta-wing tests in the 18 in. × 14 in. Tunnel for which pitching moment derivatives have only been measured for axes $x_0 = 0{\cdot}31\bar{c}$, $x_0 = 1{\cdot}04\bar{c}$, and derivatives about $x_0 = 0{\cdot}65\bar{c}$ are estimated for comparison with results from the other three tunnels.

Corrections for the effects of wind-tunnel interference on the derivatives at subsonic Mach numbers less than 0·87 have been calculated by application of equations (58) of Ref. 4. To do this, interference-free rotary derivatives l_q and m_q are required. These cannot easily be measured, but for the simple half-wing models tested, theoretical values can be used with a reasonable degree of confidence. For the half-models used in the measurements the side-wall boundary layer will reduce the lift from its value for the equivalent full wing, as will be discussed more fully in Section 4.1. The measured derivatives corrected for ventilated wall interference therefore relate to a half-model with side-wall boundary layer and not to a complete wing. The values of l_q and m_q required in the calculations should likewise be appropriate to the model with boundary layer. Although the boundary-layer correction to these derivatives is not known, the magnitude of l_q or m_q would not be expected to change by more than 15 per cent. This means that corresponding changes in the interference corrections are likely to be at most only one or two per cent since terms involving the rotary derivatives are of second order of magnitude.

The measured and estimated derivatives appropriate to the four tunnels are presented in Tables 3 to 11 and Tables 18 to 20. Equations (58) of Ref. 4 have been programmed in ALGOL for use on KDF9, and corrections for wind-tunnel interference have been obtained at six Mach numbers. At Mach numbers 0·4, 0·5, 0·6, 0·8 the theoretical values of l_q and m_q are interpolated from exact results; at $M = 0{\cdot}661$ and 0·866, l_q and m_q are known and the experimental results are interpolated to give the corrected derivatives in Tables 12 to 17, and Tables 21 and 22.

4. *Discussion.*

It is convenient to discuss results at subsonic speeds separately in Section 4.1 because at Mach numbers up to 0·85, a simple test for *large* interference effects is to compare measurements made in a ventilated tunnel with measurements made in the same tunnel with sealed walls. Derivatives measured at subsonic speeds for a half-delta model mounted in four transonic tunnels are examined in order to investigate possible changes due to the presence of the side-wall boundary layer. To confirm the suggestion in Ref. 4 that dynamic measurements in some perforated tunnels might be subject to large interference effects, further results for a symmetrically tapered wing pitching in the 25 in. × 20 in. Tunnel are discussed. In Section 4.2, a comparison of measurements at transonic speeds in the four tunnels shows that large interference effects may persist to low supersonic speeds, i.e. at least up to $M = 1{\cdot}1$. The Mach number range can be extended in the flexible wall 25 in. × 20 in. Tunnel, and in Section 4.3 it is shown that the measured lift damping derivative l_θ for the symmetrically tapered wing is subject to wall interference at Mach numbers as high as $M = 1{\cdot}35$.

4.1. *Subsonic Interference* ($M < 0{\cdot}9$).

In this section only, for the sake of brevity the term 'ventilation effect' is used to denote the change in the measured value of a derivative due to sealing the ventilated walls of a tunnel, and in Fig. 4 the effects on the derived lift damping derivatives l_θ for the half-delta model pitching about the rearmost axis in four different tunnels are plotted against Mach number. Fig. 5 shows the same results corrected for wind-tunnel interference according to equations (58) of Ref. 4. It might be recalled here that these equations are formulated on the basic assumptions that the wing and frequency parameter are both small, and that the ventilated wall behaves effectively like an open boundary. The large ventilation effect measured in the $9\frac{1}{2}$ in. × $9\frac{1}{2}$ in. Tunnel is expected since this tunnel has the largest breadth/height ratio and a model area/tunnel area ratio which is more than twice that in the other tunnels. When corrected

for interference, the difference between the two curves for the $9\frac{1}{2}$ in. × $9\frac{1}{2}$ in. Tunnel is drastically reduced but does not become zero. Part of this discrepancy may possibly arise because derivatives for the most forward pitching axis are used in the derivation of l_θ; it is already known[4] that the theory gives inaccurate corrections for damping derivatives for the particular configuration in the $9\frac{1}{2}$ in. × $9\frac{1}{2}$ in. Tunnel where the relatively large $A = 2{\cdot}64$ delta model pitches about a forward axis. In the 36 in. × 14 in. Tunnel, the measured results show little ventilation effect for $M \leqslant 0{\cdot}8$, which confirms previous observations with the symmetrically tapered wing. It is thought that in this case viscous effects in the relatively narrow slots reduce the porosity of the slotted walls which then behave more like sealed walls until $M > 0{\cdot}8$. Consequently, errors are present when results measured at low subsonic speeds in the 36 in. × 14 in. slotted Tunnel are corrected as if no viscous effects are present. This is seen in Fig. 5 where the corrected slotted-wall results are noticeably less positive than the corrected sealed results. A similar effect, but to a lesser extent, is found in the 18 in. × 14 in. Tunnel where the viscous effects are expected to be smaller than those in the 36 in. × 14 in. Tunnel; the slotted-wall interference approaches the predicted value and the overcorrection in Fig. 5 is correspondingly less. These overcorrections must be borne in mind when making comparisons between corrected results from the four ventilated tunnels.

A further type of interference was noticed in the 25 in. × 20 in. Perforated Tunnel. This tunnel is constructed so that the diffuser suction to the plenum chamber is controlled by a flap which varies the exit area from the plenum chamber to the diffuser. The tunnel has been extensively calibrated for use in steady flow tests, and a flap setting leaving a 1 in. depth of plenum chamber open to the diffuser had been chosen principally on flow stability considerations. As seen in Fig. 4, dynamic measurements in the tunnel leaving a 1 in. gap produce results which approach those for a closed tunnel as the Mach number is increased. Opening the gap to $2\frac{1}{2}$ in. has a negligible effect on the Mach number distribution down the working section, but when this adjustment is made the results are consistent with the more usual behaviour in that the ventilation effect increases with Mach number. Moreover the walls then behave almost as if they are open boundaries since the perforated tunnel results corrected on this basis are coincident with the corrected sealed tunnel results in Fig. 5. The effect of a reduction in plenum chamber suction is further shown in Fig. 6 where the pitching-damping derivative m_θ about two pitching axes is plotted against Mach number. Little effect on the stiffness derivative m_θ was observed (*see* Table 5), but the difference between the closed-tunnel values and those predicted for the tunnel with open roof and floor is so small that comparable effects would not be revealed. A disturbing feature of the changes induced in the damping derivatives is that, as for the forward axis in Fig. 6, the curves for the 1 in. flap settings sometimes cross the closed-tunnel curves against Mach number. Where the curves do not cross, the results with the smaller gap seem consistent with a boundary-layer effect following Goethert[1] who reports that the presence of a thick boundary layer seriously impairs the behaviour of perforated walls. In the present case, at Mach numbers $M \leqslant 0{\cdot}5$ diffuser suction may be sufficient to thin the boundary layer on the perforated wall in which case the tunnel behaves like an open boundary. As the Mach number increases, diffuser suction may then become insufficient and the boundary layer become thick relative to perforation size in which case the walls behave more like solid walls. But at worst, the curves for perforated and sealed walls should do no more than coincide. However, Goethert also reports that in steady flow incorrect plenum-chamber suction may produce concentrated local disturbances at the downstream end of the test section. It may be possible that in oscillatory flow such disturbances are propagated upstream to add to the boundary-layer effect and cause the observed crossing of the perforated and closed wall results. This must remain supposition until the tunnel becomes available for a detailed investigation of the cause of the discrepancies. Although the mechanism which causes these changes in the in-quadrature derivatives has not been established, it appears to be associated with insufficient plenum chamber suction. If this is increased, e.g. by opening the diffuser flaps as in the present case, the perforated walls behave in their predicted manner. A corollary to this observation is that it might be possible to control plenum chamber diffuser suction in such a way that interference-free damping derivatives would be obtained.

It is apparent that the application of corrections does not lead to a collapse of the values from the four tunnels as can be seen from the superimposed corrected and uncorrected lift derivatives in Figs. 7a to 8b. On the contrary, from Fig. 7a, it is also evident that the spread of the values of l_θ measured in the ventilated

tunnels is increased when the results are corrected for wall interference. Small errors in the results from the 36 in. × 14 in. Tunnel and the 18 in. × 14 in. Tunnel are present due to the 'overcorrections' mentioned earlier, but their effect on the spread of the results and on the relative positions of the curves is negligible. Despite the increased differences, after application of corrections for wall interference a general pattern of results tends to emerge in which it can be seen that the results from the 36 in. × 14 in. Tunnel (which has the thickest side-wall boundary layer) are usually displaced most from the interference-free values. The trend of changes due to variations in the displacement thickness of the side-wall boundary layer can be seen in the cross-plots in Fig. 9. Lift and pitching-moment derivatives in each tunnel both with sealed and ventilated walls have been corrected for wall interference at $M = 0{\cdot}8$ and plotted against the displacement thickness of the side-wall boundary layer. It is clear that the mean values of the corrected derivatives from sealed and ventilated tunnels tend to become more displaced from their interference-free values as the displacement thickness increases. This tendency is in agreement with the suggestion in Ref. 4 that values of derivatives measured with half-models are displaced from the predicted tunnel values due to the presence of the side-wall boundary layer, and is also consistent with results from steady flow[7] where loss of lift on half-models is attributed to the presence of the wall boundary layer. To get a rough estimate of the boundary-layer effect on the in-phase derivatives, one might assume that the measured lift and pitching moment relate to inviscid flow over the half-wing with its span reduced by the displacement thickness of the boundary layer. Derivatives l_θ and m_θ will thus be increased in magnitude because before adjustment, the lift and pitching moment are non-dimensionalised with respect to the actual dimensions of the model. After making adjustments for boundary-layer thickness in the suggested way and applying corrections for tunnel wall interference, it is seen in Fig. 9 that the derivatives obtained are in reasonable agreement in all tunnels and are as close as could be expected to interference-free theory for the complete model. The effect on the damping derivatives is more complicated, and there is insufficient information available to determine a simple empirical method of correction. As a further test of the trend of side-wall boundary layer effects, a $\frac{1}{2}$ in. step was fixed to the upstream end of the solid wall on which the model was mounted in the $9\frac{1}{2}$ in. × $9\frac{1}{2}$ in. Tunnel. As this was only intended as a crude qualitative test, no attempt was made to improve the very poor Mach number distribution thus produced – the Mach number being taken as the mean value in the vicinity of the model. Boundary layer traverses indicated that the boundary-layer thickness at the position of the model had been increased from the small value 0·7 in. to 3·0 in. at $M = 0{\cdot}6$ which is roughly of the same order as the boundary-layer thickness in the 36 in. × 14 in. Tunnel. As shown in Fig. 7a, the in-phase lift derivative l_θ is displaced in the expected manner. Attaching the step also causes substantial changes at low Mach numbers in the lift damping $l_{\dot\theta}$ (Fig. 8a) so that it is displaced towards the values in the large tunnels, but the changes appear to decrease as the Mach number increases. However, the magnitude of the displacement, particularly at high Mach numbers, should be regarded with suspicion in view of the poor Mach-number distribution down the tunnel. It is possible that the lift damping derivative $l_{\dot\theta}$ is more sensitive than the in-phase lift derivative l_θ to any gradients present, and that this causes the unexpected variation of $l_{\dot\theta}$ with Mach number. It might be noted here that the actual boundary-layer thickness in the 36 in. × 14 in. Tunnel is of the same order as the span of the half-delta model. Even with this abnormal configuration, it is seen in Fig. 9 for instance that discrepancies in the measured derivatives after correction for tunnel-wall interference are not excessive. It appears that for a more practical situation as in the case of the half-delta model in the $9\frac{1}{2}$ in. × $9\frac{1}{2}$ in. Tunnel, the discrepancies may be acceptably small so that the effect of the side-wall boundary layer can be ignored.

When the 25 in. × 20 in. Tunnel had slotted walls, large ventilation effects on the damping derivatives were measured on testing half-models of symmetrically tapered and M-wing planforms. The theory of Ref. 4 explained the results satisfactorily and gave reason to believe that the present perforated walls with large open area ratio (20 per cent) might also produce large ventilation effects. Tests on the unswept tapered wing have recently been repeated in the perforated tunnel. Fig. 10 shows the variation of pitching damping with Mach number for a pitching axis to the rear of the centre of pressure with slotted walls, with perforated walls and with walls sealed. Agreement between the two sets of sealed tunnel results is reasonable. Although the ventilation effect in the perforated tunnel is significantly large, it appears to be less than that in the slotted tunnel except at the lower Mach numbers where $M \leqslant 0{\cdot}6$, and apparently

does not become of the same order again until $M \approx 1{\cdot}05$. However, the tests were completed before the discovery of the diffuser suction effect discussed earlier and the standard 1 in. flap setting was used. The divergence of the perforated results from the slotted results for $M > 0{\cdot}6$ is of the same form as the trend observed for oscillations about the rearward axis of the delta wing when the flap setting is reduced from $2\frac{1}{2}$ in. to 1 in. It follows that a $2\frac{1}{2}$ in. flap setting would probably have produced results of the same order as those in the slotted tunnel for all Mach numbers. The large effects observed with the tapered wing are consistent with the tests on the delta wing since these produced changes in l_θ of order 35 per cent on sealing the perforated walls (Fig. 4), even though the ratio of model area to tunnel area was as small as 0·024.

During the tests on the tapered wing, the perforations were progressively sealed in streamwise strips in order to reduce the porosity of the ventilated walls. A slot parameter was thus introduced because in essence, each wall was ventilated as if perforations had been fitted over four longitudinal slots. When 55 per cent of the perforated wall was sealed in this way, the remaining perforations gave an open area ratio of 8·9 per cent which was nearly equal to the 9·1 per cent open area of the original slotted walls. The small changes shown in Fig. 11 are therefore probably due to the associated small change in slot parameter F from 0 to 0·09. Further sealing to leave 13 per cent of the perforations open drastically reduces the ventilation effect giving results close to the sealed tunnel results. In this case, the slot parameter has a value $F = 0{\cdot}27$. Comparison with results obtained when the 25 in. × 20 in. Tunnel had a slotted roof and floor shows that this increase in the value of the slot parameter would not alone produce such a large reduction in interference. It follows that there is now a significant porosity effect causing the four 'perforated slots' to behave in a similar way to the slotted walls in the 36 in. × 14 in. Tunnel where viscous effects reduce the porosity of the walls. Porosity effects in steady flow have been described through a parameter β/P which is zero for a completely open boundary and infinite for a closed boundary. The effect of β/P in unsteady flow and its variation with open area ratio for a perforated wall has not yet been established; if β/P has a similar effect to that in steady flow in Fig. 2 of Ref. 4, then a mean value of P of approximately 0·3 for the case where $F = 0{\cdot}27$ would explain the present results.

4.2. *Transonic Interference* ($0{\cdot}9 \leqslant M \leqslant 1{\cdot}1$).

The measured pitching-moment derivatives and deduced lift derivatives for the half-delta model are plotted against Mach number for three pitching axes in Figs. 12 to 15c. Results from the four transonic tunnels are superimposed in order to detect any substantial differences between the curves. In the previous Section, it is shown that the major part of the difference between the lift derivative l_θ from the tests in the $9\frac{1}{2}$ in. × $9\frac{1}{2}$ in. Tunnel and those in the other tunnels is due to ventilated-wall interference. From Figs. 13a to 13c it is clear that the interference extends into the transonic speed range. At sonic speed for instance, the values of the damping derivatives in the $9\frac{1}{2}$ in. × $9\frac{1}{2}$ in. Tunnel are too far removed from the results in the other tunnels to be attributable solely to a side-wall boundary-layer effect, especially as there is little difference between the results in the 36 in. × 14 in. Tunnel and in the 18 in. × 14 in. Tunnel although the relative thicknesses of the boundary layers are nearly 2 to 1. Changes in the stiffness derivatives l_θ, m_θ show similar trends but on a much smaller scale (Figs. 12, 14a to 14c). The pitching damping derivative $m_{\dot\theta}$ is seen in Figs. 15a to 15c to be subject to large effects which continue up to $M = 1{\cdot}1$, but these are sometimes difficult to interpret. The interference on pitching damping tends to change in magnitude and sign with axis position according to the value of the derivative $m_{\dot\theta}$. Since the centre axis for the half-delta-model passes close to the aerodynamic centre at subsonic speeds, $m_{\dot\theta}$ is very small and interference effects on $m_{\dot\theta}$ are negligible (Fig. 15b). At transonic speeds, the position of the aerodynamic centre moves downstream as indicated by the negative values of $m_{\dot\theta}$, and interference effects on $m_{\dot\theta}$ of the same form as for an upstream pitching axis (Fig. 14a) are therefore expected. One sees in Fig. 14b that such effects do occur for tests with the centre axis at Mach numbers above 0·9, although the increase in damping measured in the $9\frac{1}{2}$ in. × $9\frac{1}{2}$ in. Tunnel compared with the damping in the other tunnels seems rather large considering the relatively small change in position of the aerodynamic centre. For the forward pitching axis in Fig. 15a, the large effect at subsonic speeds continues through the transonic speed range in a similar way to the effect on l_θ at all pitching axis positions.

Measured derivatives for the symmetrically tapered wing in the 36 in. × 14 in. Slotted Tunnel and the 25 in. × 20 in. Perforated Tunnel are shown in Figs. 16 to 19c. It is unfortunate that the behaviour

of these two tunnels in the transonic speed range is not fully understood. The 36 in. × 14 in. Tunnel has been shown to behave more like a sealed tunnel at low subsonic speeds ($M < 0{\cdot}8$) probably due to viscous effects in the slots which, according to linearized theory, may be described by a parameter β/P where the porosity parameter P is unknown. It is therefore possible, but not established, that the viscous effects become small near sonic speed. All the results in the perforated tunnel were obtained with the 1 in. flap setting which has been shown to have a significant effect at subsonic speeds. However, its effect at transonic speeds is open to question so there is no satisfactory datum at transonic speeds with which to compare the results from either tunnel. Results measured with the ventilations sealed are shown at Mach numbers less than 0·85. The differences between the two sealed tunnels are in accordance with interference theory, and arise because the nearly square effective cross-section of the 36 in. × 14 in. Tunnel has a greater interference effect for sealed walls than the effective duplex shape of the 25 in. × 20 in. Tunnel. In Figs. 16, 17, 19b and 19c in particular, it can be seen that the difference between the results in the 25 in. × 20 in. Tunnel with perforated walls and the results obtained when the walls are sealed is still large at $M = 0{\cdot}85$ and there is no tendency for the difference to become signficantly smaller with increasing Mach number. Since the bulk of this difference at subsonic speeds is due to perforated wall interference, it appears likely that there will be wall interference present when testing in the transonic speed range. There is further evidence from a direct comparison of the results in the two ventilated tunnels at transonic speeds. As discussed in Ref. 4, the 36 in. × 14 in. Slotted Tunnel at $M \geqslant 0{\cdot}85$ is likely either to give results close to the interference-free values, or it may behave as if it has an open roof and floor. Since the value of the in-phase lift derivative l_θ is decreased when measured in a tunnel with an roof and floor, the results in the 36 in. × 14 in. Tunnel shown in Fig. 16 are likely to be either interference free or below the interference-free values. At speeds $M < 1{\cdot}1$ the results from the 25 in. × 20 in. Perforated Tunnel are still lower indicating that there is interference present. In a similar way, since the lift damping derivative $l_{\dot\theta}$ is increased (in the sense of making it more positive) when measured in a tunnel with open roof and floor, the results for the 36 in. × 14 in. Tunnel shown in Fig. 17 are likely to be either interference free or above the interference-free values. The results in the 25 in. × 20 in. Perforated Tunnel are still higher when $M < 1{\cdot}1$. The behaviour of the pitching damping derivative in Fig. 19 is also consistent with the presence of wall interference since, by comparison with wall effects at subsonic speeds, the damping is expected to increase when the pitching axis is upstream of the aerodynamic centre and decrease when the axis is downstream of the aerodynamic centre. For the upstream axis in Fig. 19a the measured damping in the 25 in. × 20 in. Tunnel is larger than that in the 36 in. × 14 in. Tunnel, and the opposite trend is seen for the downstream axis in Figs. 19b and 19c. The trend in the measured values of m_θ in Fig. 18 is not as clearly defined, but the results are also consistent because the effect of a tunnel with an open roof and floor is to decrease the value of $|m_\theta|$ although only small changes are expected. It therefore follows that there is wall interference present on measurements made in the 25 in. × 20 in. Tunnel at transonic speeds, but no conclusion can be drawn regarding the 36 in. × 14 in. Tunnel since (again by comparison with effects at subsonic speeds) greater interference is expected in the 25 in. × 20 in. Tunnel even if the slotted walls of the 36 in. × 14 in. Tunnel behave like open boundaries to give an interference effect which is not negligible.

Ventilated wall interference at subsonic speeds is associated with wall constraint on the upwash propagated upstream to the oscillating model. One would therefore expect the interference to become small at transonic speeds because no disturbances can be propagated directly upstream once supersonic flow has been achieved. Since wall effects are not small in the present case, one seeks a different mechanism by which interference upwash can be propagated upstream at low supersonic speeds. The obvious path is *via* the plenum chamber. With steady flow, Ref. 1 reports upstream effects in supersonic flow in a slotted tunnel due to secondary flow within the slots: in unsteady flow, it is possible that these effects may be propagated upstream to influence the main supersonic flow. Induced upwash ahead of a wing performing pitching oscillations in a slotted tunnel has recently been measured directly[5], and with slots open, model induced upwash was observed at speeds as high as $M = 1{\cdot}14$. The variation of this induced upwash with Mach number is reproduced in Fig. 20. With slots sealed, the upwash tends to zero as sonic speed is approached as would be expected, but at $M = 1{\cdot}14$, the upwash at 1·04 root chords upstream of the model axis with slots open is of the same order as that measured at subsonic speeds. However, when the slots

were sealed from the upstream end of the working section to a point just downstream of the measuring position no upwash could be detected at supersonic speeds. Additional measurements showed that pressure fluctuations associated with the oscillating model were negligible in the body of the plenum chamber but appreciable fluctuations occurred close to the slotted wall. These tests suggest that the induced upwash at supersonic speeds is caused by disturbances propagated upstream in the region of the slotted wall. The limited evidence from the tests in the perforated 25 in. × 20 in. Tunnel indicates that upstream propagation can also occur with a perforated wall. Presumably, the same mechanism exists at subsonic speeds, but in view of the successful predictions of the subsonic theory[4] which ignores contributions from this source, the additional interference upwash produced is probably small. As the Mach number is increased the additional upwash is likely to become more dominant until at low supersonic speeds, there is no direct induced upwash ahead of the model but the upwash due to the upstream propagation near the ventilated wall is of comparable magnitude to the upwash in subsonic flow. Of course, the upwash measured at subsonic speeds is the sum of interference upwash and that due to the wing itself, whilst that measured at supersonic speeds is interference upwash only. Nevertheless, since these appear to be of the same order in Fig. 20, it is interesting to examine the consequences of applying the method of correction formulated for subsonic speeds to the present results at transonic speeds. Some modification is necessary because the theoretical corrections are proportional to $1/\beta$. From Fig. 13 for instance, it would appear that a constant correction of the same order as that at $M \approx 0{\cdot}89$ is required throughout the transonic speed range. It is therefore convenient to fix the value of β to be 0·45 and calculate corrections to the measured derivatives from equations (70) of Ref. 4. The crudest method of correction has to be used because there are no reliable theoretical values of rotary derivatives l_q and m_q at these speeds. The corrected lift and pitching-moment derivatives for the delta-wing pitching about its most rearward axis position are shown in Figs. 21 to 24; corrected derivatives for the other two pitching axes are presented in Tables 12 to 17. Although the spread of the results has not improved in some cases, with consideration of the side-wall boundary-layer effects as discussed earlier, it appears that the empirical correction improves the correlation between results in the four tunnels throughout the transonic speed range. The same method of correction has been applied to the derivatives for the tapered wing in the 25 in. × 20 in. Perforated Tunnel and the 36 in. × 14 in. Slotted Tunnel, and the differences in the results for Mach numbers $M < 1{\cdot}1$ tend to be reduced as seen in Table 22. Here, one must recall that whilst no side-wall boundary-layer effects are expected, it is not certain that the viscous effects at the ventilated walls in these tunnels become small at transonic speeds. However, since application of the method of correction appears to give some general improvement in the comparisons of results from different tunnels, it is suggested that if significant ventilated-wall interference effects are present at subsonic speeds and these cannot be suitably reduced by modifying the experimental configuration, then one should calculate the subsonic corrections until $M \approx 0{\cdot}89$ and use $\beta = 0{\cdot}45$ say in the transonic range until $M \approx 1{\cdot}10$.

Finally, two points might be noted. Firstly, it is shown in Ref. 5 that the upstream propagation at $M = 1{\cdot}14$ can be damped out by fitting perforated screens behind the slots. The same screens also drastically reduce the subsonic interference through their effect on the porosity of the slotted walls. Secondly, large interference effects at transonic speeds have only been observed when those at subsonic speeds are also large. It has yet to be established whether substantial effects at transonic and low supersonic speeds can exist in tunnels giving no interference at subsonic speeds.

4.3. *Supersonic Interference* ($M > 1{\cdot}1$).

The perforated 25 in. × 20 in. Tunnel has flexible liners with which Mach numbers up to $M = 1{\cdot}6$ can be achieved. Figs. 16 to 19c include the measured pitching moment and lift derivatives for the symmetrically tapered planform in the range $1{\cdot}1 \leqslant M \leqslant 1{\cdot}4$. The curves for the pitching moment derivatives agree reasonably well with supersonic theory[8] for $M > 1{\cdot}3$ and with derivatives measured in a tunnel with solid liners[9]. In view of this agreement, the theory would be expected to predict reasonably accurate values of the lift derivatives under the same conditions. However, whilst the relative differences in the in-phase lift are small, there is a significant discrepancy between the measured and predicted lift damping. At $M = 1{\cdot}36$, for instance, the measured value 2·52 is 81 per cent more negative than theory. Simple tests

were done to show that this is a perforated wall effect. The perforations were sealed from the upstream end of the working section so that the first Mach line from the start of the perforations passed:

(i) just upstream of the model leading edge,

(ii) through the centreline of the model,

(iii) just downstream of the model trailing edge.

Hence, in case (iii) any effect associated with the plenum chamber or perforated wall could not be felt by the model. By progressively sealing the wall in this way, the Mach-number distribution down the working section was changed. Careful calibration showed that the Mach-number distribution in the region of the model was different but reasonably uniform in each case. With configuration (i) there was no change in the measured lift damping derivative but, as seen in Fig. 25, with (ii) $l_{\dot{\theta}}$ was displaced nearly one third of the distance from the experimental curve for the perforated tunnel towards the theoretical curve with allowance for aerofoil thickness; with (iii) it was displaced by over half of the original discrepancy. Corresponding changes in $m_{\dot{\theta}}$ were small and inconsistent. However, the value of $m_{\dot{\theta}}$ was so small that similar effects might not be detected. No changes in l_{θ} or m_{θ} were evident.

The part-sealing tests show that there is some upstream propagation of disturbances in the perforated tunnel at quite high supersonic speeds. Although the effect is only measurable on $l_{\dot{\theta}}$, this is sufficient to show that great care must be taken when interpreting dynamic measurements in ventilated tunnels even with supersonic flow. If possible, steps should be taken to ensure that there is no upstream propagation of disturbances. In a slotted tunnel, suitable perforated screens placed behind the slots appear to do this: with perforated tunnels, a reduction in the porosity of the perforated wall will probably be the answer.

5. *Summary of Conclusions.*

(a) It is shown that, if large interference effects on dynamic measurements in ventilated tunnels are present at subsonic speeds, they are likely to persist to low supersonic speeds. Evidence is presented which suggests that the interference at low supersonic speeds is due to an upstream propagation of disturbances in the plenum chamber near to the ventilated wall. It is not established whether significant transonic interference will occur in ventilated tunnels which are free from interference at subsonic speeds.

(b) Tests in a tunnel which has a perforated roof and floor show that perforated-wall interference can be as large as interference in a slotted tunnel. Furthermore, limited evidence from the measurement of lift damping for the symmetrically tapered wing indicates that interference in this tunnel persists up to a Mach number $M = 1{\cdot}35$. The perforated walls with 20 per cent open area ratio probably have high posority, and it is possible that less porous walls would give less interference.

(c) The diffuser suction applied to the plenum chambers in the perforated tunnel can be controlled by adjustable flaps at the downstream end of the working section. It is found that the in-quadrature dervatives $l_{\dot{\theta}}$, $m_{\dot{\theta}}$ are particularly sensitive to the position of the flaps. When the exit area from the plenum chambers to the diffuser is too small, the derivatives for $M \geqslant 0{\cdot}6$ fall away from the open roof and floor values towards the sealed tunnel values. In some cases, the curves against Mach number of derivatives in the perforated tunnel and derivatives in the sealed tunnel cross over, and further experiments would be needed to discover the reason.

(d) It is shown that the thickness of the side-wall boundary layer in which the half-model is immersed systematically influences all the derivatives. When the boundary-layer thickness is relatively large compared with model span and the model/tunnel area ratio is small, the changes in the derivatives are of the same order of magnitude as the changes due to wind-tunnel interference. This confirms the suggestion in Ref. 4 that wind-tunnel interference cannot be reduced to negligible proportions simply by reducing the size of the half-model because the boundary-layer effect would become dominant. However, the tests on the half-delta-model show that when the ratio of model area to tunnel area is not less than 0·08 say, the boundary-layer effect might be acceptably small.

6. *Further Work.*

Although it has been shown that dynamic measurements in ventilated tunnels may be subject to wall

interference at transonic speeds, the picture is still far from clear. A reliable interference-free datum seems to be essential and the simplest way to obtain this as an extension to the tests described in this Report might be to use the small half-delta model in the relatively large 36 in. × 14 in. Tunnel with the side-wall boundary layer removed or drastically thinned. In this way, any doubts as to the effect of the side-wall boundary layer are removed and the slotted-wall interference is small primarily because a small value of the ratio model area/tunnel area is obtained. Further work is necessary to establish whether the criteria for the reduction of subsonic ventilated wall interference will in general simultaneously reduce the transonic interference which appears to involve a different mechanism. It is known[5] that in some cases interference at both subsonic and transonic speeds in slotted tunnels may be substantially reduced by fitting suitable perforated screens in the plenum chamber. An understanding of the action of such screens may follow from a current experimental investigation at NPL, in which screens of variable porosity have been incorporated in the $9\frac{1}{2}$ in. × $9\frac{1}{2}$ in. Slotted Tunnel. The results might indicate an empirical method for prevention of transonic interference, but a most desirable complement would be a soundly based theoretical method for prediction and correction of interference effects at transonic speeds. A further investigation of the diffuser suction effect noticed in the 25 in. × 20 in. Perforated Tunnel is desirable in order to understand exactly what causes the changes in the damping derivatives.

7. *Acknowledgements.*

The authors wish to acknowledge the valuable assistance of Mrs. J. A. Moreton in obtaining the results, and for the ALGOL programmes she wrote for the reduction of measurements and interference calculations. Acknowledgement is also due to Mr. H. C. Garner for many helpful discussions. Staff of the model-making department of Aerodynamics Division, NPL supplied the half-wings used in the experiments.

LIST OF SYMBOLS

a	Slot width
b	Breadth of tunnel working section
$\bar{c}$	Mean Chord of model half-wing
C	Cross-sectional area of tunnel working section $= bh$
$\bar{C}_L$	(Complex lift)/$\frac{1}{2}\rho U^2 S$
$\bar{C}_m$	(Complex pitching moment)/$\frac{1}{2}\rho U^2 S\bar{c}$
d	Slot spacing
F	Slot parameter $= \frac{2d}{\pi h}\log_e \operatorname{cosec}\frac{\pi a}{2d}$
h	Height of tunnel working section
M	Mach number
P	Porosity parameter for a ventilated wall
δp	Pressure drop across ventilated wall $= \frac{\rho U}{P} v_n$
s	Span of model half-wing
S	Area of model half-wing $= s\bar{c}$
U	Velocity of undisturbed stream
v_n	Velocity normal to ventilated wall
x_0	Streamwise distance of pitching axis from the root chord leading edge

z_0	Amplitude of heaving oscillation
β	$\sqrt{\lvert 1-M^2 \rvert}$
θ_0	Amplitude of pitching oscillation
$\bar{\nu}$	Frequency parameter $= \omega \bar{c}/U$
ρ	Density of undisturbed stream
ω	Angular frequency of oscillation

Derivatives.

The non-dimensional derivatives of lift l_θ, $l_{\dot{\theta}}$, l_z, $l_{\dot{z}}$ are defined by

$$\bar{C}_L = 2\,\theta_0\,(l_\theta + i\bar{\nu}\,l_{\dot{\theta}}) + 2\frac{z_0}{\bar{c}}(l_z + i\bar{\nu}\,l_{\dot{z}})$$

The non-dimensional derivatives of pitching moment m_θ, $m_{\dot{\theta}}$, m_z, $m_{\dot{z}}$ are defined by

$$\bar{C}_m = 2\,\theta_0\,(m_\theta + i\bar{\nu}\,m_{\dot{\theta}}) + 2\frac{z_0}{\bar{c}}(m_z + i\bar{\nu}\,m_{\dot{z}})$$

Derivatives l_q and m_q are the non-dimensional lift and pitching moment associated with steady rotary pitching motion. If the angular velocity of the rotary motion is $q = i\omega\,\theta_0$ then, to first order in frequency parameter, l_q and m_q are given by the relations

$$\bar{C}_L = 2\,i\,\theta_0\,\bar{\nu}\,l_q$$

$$\bar{C}_m = 2\,i\,\theta_0\,\bar{\nu}\,m_q$$

Suffices.

The suffices 1, 2, 3 used in tabulating the results refer to the upstream axis, the centre axis, and the downstream axis respectively for each model: the axis positions are given in Section 2.

REFERENCES

No.	*Author(s)*	*Title, etc.*
1	B. H. Goethert	Transonic Wind Tunnel Testing. AGARDograph 49. Pergamon Press. 1961.
2	E. W. E. Rogers	Wall interference in tunnels with ventilated walls. Subsonic Wind Tunnel Wall Corrections (ed. H. C. Garner), Chap. VI. AGARDograph 109. 1967.
3	K. C. Wight	A review of slotted-wall wind-tunnel interference effects on oscillating models in subsonic and transonic flows. *J. R. aero. Soc.* Vol. 68, pp. 670–674. 1964.
4	H. C. Garner, A. W. Moore and K. C. Wight ..	The theory of interference effects on dynamic measurements in slotted-wall tunnels at subsonic speeds and comparisons with experiment. A.R.C. R. & M. 3500. September 1966.
5	G. Q. Hall and J. S. Claridge	Measurements of flow disturbances caused by an oscillating wing in a slotted wall tunnel. H.S.D./Cov. A.R. Report No. 66/4. October 1966.
6	J. B. Bratt	A note on derivative apparatus for the NPL $9\frac{1}{2}$ inch high-speed tunnel. A.R.C. C.P. 269. January 1956.
7	K. J. Orlik-Rückemann and J. G. Laberge ..	Static and dynamic longitudinal stability characteristics of a series of delta and swept-back wings at supersonic speeds. N.R.C. (Canada) Aero. Report LR–396. January 1966.
8	Doris E. Lehrian	Calculation of stability derivatives for tapered wings of hexagonal planform oscillating in a supersonic stream. A.R.C. R. & M. 3298. September 1960.
9	L. Woodgate, J. F. M. Maybrey and C. Scruton	Measurement of pitching-moment derivatives for rigid tapered wings of hexagonal planform oscillating in supersonic flow. A.R.C. R. & M. 3294. March 1961.

TABLE 2*

Nominal Tunnel Size	$9\frac{1}{2}$ in. × $9\frac{1}{2}$ in.	18 in. × 14 in.	25 in. × 20 in.		36 in. × 14 in.
			Slotted	Perforated	
Length of ventilated wall	2·42 ft (0·74m)	5·46 ft (1·66m)	8·00 ft (2·44m)	3·79 ft (1·16m)	9·00 ft (2·74m)
Length of ventilated wall downstream of model axis	1·04 ft (0·32m)	2·46 ft (0·75m)	3·75 ft (1·14m)	1·83 ft (0·56m) with delta wing 2·50 ft (0·76m) with tapered wing	3·75 ft (1·14m)
Open area ratio	15·8%	9·1%	9·1%	20%	9·1%
Thickness of liner	0·094 in. (2·4mm)	0·04 in. (2·4mm)	0·125 in. (3·2mm)	0·125 in. (3·2mm)	0·090 in. (2·3mm)
Width of slot or Diameter of Perforation	0·094 in. (2·4mm)	0·0116 in. (2·9mm)	0·165 in. (4·2mm)	0·17 in. (4·3mm)	0·116 in. (2·9mm)
Width of slat	0·50 in. (1·27cm)	1·16 in. (2·95cm)	1·65 in. (4·19cm)	—	1·16 in (2·95cm)
Depth of plenum chamber	2·6 in. (6·6cm)	6·5 in. (16·5cm)	7·5 in (19·1cm)	7·5 in. (19·1cm)	8·5 in. (21·6cm)

*Table 1 is included in Fig. 1.

TABLE 3

Measured Derivatives for Delta Wing, $A = 2{\cdot}64$

$9\frac{1}{2}$ in. × $9\frac{1}{2}$ in. Tunnel
Slotted Tunnel

M	$-m_{\theta_1}$	$-m_{\dot{\theta}_1}$	M	m_{θ_2}	$-m_{\dot{\theta}_2}$	M	m_{θ_3}	$-m_{\dot{\theta}_3}$
0·41	0·447	1·037	0·408	0·009	0·355	0·408	0·517	0·018
0·51	0·469	1·060	0·511	0·006	0·368	0·510	0·513	0·013
0·61	0·491	1·083	0·612	0·000	0·415	0·612	0·533	0·036
0·72	0·505	1·239	0·715	−0·008	0·468	0·714	0·545	0·077
0·82	0·512	1·368	0·817	−0·007	0·553	0·817	0·559	0·179
0·87	0·549	1·502	0·869	−0·010	0·609	0·867	0·573	0·271
0·93	0·561	1·634	0·922	−0·008	0·726	0·919	0·600	0·413
0·98	0·635	2·005	0·974	−0·041	1·117	0·971	0·570	0·650
1·03	0·692	1·700	1·027	−0·065	1·248	0·998	0·543	0·708
1·09	0·790	1·322	1·081	−0·141	0·959	1·025	0·528	0·756
1·14	0·837	0·984	1·131	−0·208	0·780	1·050	0·518	0·773
						1·076	0·501	0·847
						1·127	0·466	0·893

Slots Sealed

M	$-m_{\theta_1}$	$-m_{\dot{\theta}_1}$	$-m_{\theta_2}$	$-m_{\dot{\theta}_2}$	m_{θ_3}	$-m_{\dot{\theta}_3}$
0·40	0·534	0·916	0·024	0·389	0·548	0·170
0·51	0·569	0·924	0·021	0·378	0·567	0·193
0·61	0·582	0·933	0·016	0·416	0·593	0·252
0·71	0·618	1·014	0·015	0·472	0·623	0·304
0·81	0·671	1·136	0·015	0·610	0·658	0·474

TABLE 4

Measured Derivatives for Delta Wing, A = 2·64

18 in. × 14 in. Tunnel.

M	Slotted Tunnel				Slots Sealed			
	$-m_{\theta_1}$	m_{θ_3}	$-m_{\dot{\theta}_1}$	$-m_{\dot{\theta}_3}$	$-m_{\theta_1}$	m_{θ_3}	$-m_{\dot{\theta}_1}$	$-m_{\dot{\theta}_3}$
0·40	0·515	0·526	0·861	0·148	0·515	0·525	0·824	0·198
0·50	0·511	0·528	0·871	0·176	0·522	0·550	0·826	0·224
0·60	0·528	0·545	0·896	0·221	0·537	0·570	0·841	0·288
0·70	0·534	0·562	0·943	0·292	0·569	0·594	0·884	0·362
0·80	0·579	0·586	1·001	0·417	0·609	0·626	0·959	0·540
0·85	0·590	0·605	1·068	0·505	0·646	0·665	1·028	0·679
0·90	0·624	0·630	1·199	0·694				
0·95	0·796	0·562	1·312	0·946				
1·00	0·910	0·494	0·302	0·829				
1·05	0·988	0·437	0·323	0·729				
1·10	0·971	0·411	0·087	0·761				

TABLE 5

Measured Stiffness Derivatives for Delta Wing, A = 2·64

25 in. × 20 in. Tunnel.

M	Perforated Tunnel					Perforations Sealed		
	$-m_{\theta_1}$		m_{θ_2}	m_{θ_3}		$-m_{\theta_1}$	m_{θ_2}	m_{θ_3}
	1 in. gap	$2\frac{1}{2}$ in. gap	1 in. gap	1 in. gap	$2\frac{1}{2}$ in. gap	—		
0·40	0·500	0·459	0·002	0·501	0·492	0·520	−0·009	0·526
0·50	0·507	0·492	0·001	0·515	0·518	0·527	−0·006	0·540
0·60	0·521	0·500	0·001	0·530	0·529	0·543	−0·005	0·565
0·70	0·544	0·525	0·003	0·547	0·543	0·558	−0·005	0·581
0·80	0·547	0·548	0·006	0·565	0·568	0·592	−0·006	0·610
0·85	0·582	0·560	0·004	0·586	0·590	0·600	−0·004	0·630
0·90	0·632	0·592	−0·006	0·604	0·599			
0·95	0·771	0·751	−0·045	0·568	0·567			
1·00	0·858	0·862	−0·187	0·490	0·498			
1·05	0·903		−0·247	0·454				
1·10	0·921		−0·262	0·426				
1·20	0·882		−0·297	0·338				
1·30	0·837		−0·293	0·293				
1·40	0·779		−0·284	0·259				

TABLE 6

Measured Damping Derivatives for Delta Wing, $A = 2{\cdot}64$

25 in. × 20 in. Tunnel.

M	Perforated Tunnel					Perforations Sealed		
	$-m_{\dot{\theta}_1}$		$-m_{\dot{\theta}_2}$	$-m_{\dot{\theta}_3}$		$-m_{\dot{\theta}_1}$	$-m_{\dot{\theta}_2}$	$-m_{\dot{\theta}_3}$
	1 in. gap	$2\frac{1}{2}$ in. gap	1 in. gap	1 in. gap	$2\frac{1}{2}$ in. gap	—		
0·40	0·863	0·868	0·339	0·143	0·130	0·841	0·339	0·182
0·50	0·894	0·890	0·357	0·188	0·175	0·855	0·367	0·220
0·60	0·883	0·910	0·387	0·256	0·215	0·878	0·391	0·271
0·70	0·910	0·935	0·427	0·327	0·829	0·911	0·433	0·345
0·80	0·923	1·017	0·500	0·477	0·380	0·981	0·520	0·479
0·85	0·984	1·097	0·565	0·569	0·417	1·064	0·587	0·597
0·90	1·124	1·302	0·699	0·716	0·560			
0·95	1·237	1·487	0·911	1·003	0·803			
1·00	0·382	0·588	0·477	0·913	0·758			
1·05	0·379		0·375	0·916				
1·10	0·171		0·261	0·879				
1·20	0·215		0·153	0·521				
1·30	0·279		0·156	0·423				
1·40	0·298		0·140	0·579				

TABLE 7

Measured Derivatives for Delta Wing, $A = 2{\cdot}64$

36 in. × 14 in. Tunnel

M	Slotted Tunnel						Slots Sealed					
	$-m_{\theta_1}$	$-m_{\theta_2}$	m_{θ_3}	$-m_{\dot{\theta}_1}$	$-m_{\dot{\theta}_2}$	$-m_{\dot{\theta}_3}$	$-m_{\theta_1}$	$-m_{\theta_2}$	m_{θ_3}	$-m_{\dot{\theta}_1}$	$-m_{\dot{\theta}_2}$	$-m_{\dot{\theta}_3}$
0·40	0·486	0·003	0·473	0·768	0·296	0·182	0·472	0·003	0·487	0·764	0·302	0·197
0·50	0·496	0·006	0·491	0·772	0·319	0·213	0·487	0·017	0·509	0·784	0·323	0·229
0·60	0·488	0·008	0·505	0·800	0·337	0·254	0·517	0·015	0·521	0·814	0·353	0·277
0·70	0·522	0·010	0·523	0·808	0·383	0·315	0·535	0·020	0·543	0·841	0·391	0·355
0·80	0·540	0·013	0·544	0·849	0·447	0·407	0·545	0·013	0·579	0·916	0·481	0·476
0·85	0·548	0·010	0·565	0·932	0·507	0·495	0·581	0·013	0·607	0·977	0·603	0·657
0·90	0·568	0·008	0·573	1·025	0·607	0·629						
0·95	0·658	0·074	0·548	1·236	0·828	0·906						
1·00	0·812	0·173	0·496	0·556	0·440	0·878						
1·05	0·868	0·220	0·447	0·325	0·361	0·838						
1·10	0·904	0·263	0·411	0·228	0·248	0·680						

TABLE 8

Measured Derivatives for Delta Wing in $9\frac{1}{2}$ in. × $9\frac{1}{2}$ in. Tunnel with $\frac{1}{2}$ in. Step.

M	$-m_{\theta_1}$	$-m_{\theta_2}$	m_{θ_3}	$-m_{\dot{\theta}_1}$	$-m_{\dot{\theta}_2}$	$-m_{\dot{\theta}_3}$
0·42	0·400	0·017	0·425	0·833	0·316	0·068
0·53	0·407	0·016	0·430	0·850	0·331	0·077
0·63	0·422	0·018	0·439	0·956	0·354	0·078
0·74	0·435	0·022	0·452	1·047	0·432	0·095
0·85	0·452	0·027	0·474	1·172	0·506	0·194
0·90	0·459	0·028	0·492	1·226	0·550	0·231
0·96	0·459	0·015	0·517	1·321	0·660	0·298
1·02	0·503	0·022	0·524	1·615	0·770	0·502
1·07	0·584	0·075	0·505	2·003	0·896	0·744
1·13	0·763	0·147	0·469	1·460	0·708	0·693
1·19	0·782	0·207	0·440	1·090	0·723	0·855

Calculated Lift Derivatives for Delta Wing in $9\frac{1}{2}$ in. × $9\frac{1}{2}$ in. Tunnel with $\frac{1}{2}$ in. Step.

M	l_θ	$l_{\dot{\theta}_1}$	$l_{\dot{\theta}_2}$	$l_{\dot{\theta}_3}$
0·42	1·138	1·492	1·095	0·642
0·53	1·154	1·501	1·104	0·653
0·63	1·188	1·700	1·252	0·745
0·74	1·224	1·775	1·350	0·866
0·85	1·277	1·876	1·395	0·841
0·90	1·310	1·911	1·424	0·857
0·96	1·345	1·927	1·470	0·939
1·02	1·416	2·260	1·600	0·854
1·07	1·501	2·709	1·784	0·737
1·13	1·704	1·795	0·939	0·055
1·19	1·685	0·818	0·197	−0·504

TABLE 9

Calculated Lift Derivatives for Delta Wing A = 2·64

M	$9\frac{1}{2}$ in. × $9\frac{1}{2}$ in. Slotted Tunnel				M	18 in. × 14 in. Slotted Tunnel			
	l_θ	$l_{\dot\theta_1}$	$l_{\dot\theta_2}$	$l_{\dot\theta_3}$		l_θ	$l_{\dot\theta_1}$	$l_{\dot\theta_2}$	$l_{\dot\theta_3}$
0·41	1·322	1·914	1·560	0·949	0·40	1·426	1·503	1·020	0·462
0·51	1·346	1·948	1·567	0·966	0·50	1·423	1·480	0·999	0·441
0·61	1·402	1·968	1·475	0·944	0·60	1·470	1·470	0·972	0·398
0·72	1·438	2·136	1·762	1·087	0·70	1·501	1·454	0·945	0·358
0·82	1·467	2·187	1·885	1·116	0·80	1·596	1·386	0·846	0·221
0·87	1·536	2·259	2·078	1·138	0·85	1·637	1·376	0·820	0·181
0·92	1·591	2·273	2·108	1·111	0·90	1·718	1·322	0·738	0·068
0·98	1·651	2·426	1·978	1·221	0·95	1·860	1·063	0·429	−0·295
1·03	1·671	1·821	0·636	0·601	1·00	1·923	−0·228	−0·898	−1·632
1·08	1·769	1·152	0·277	−0·140	1·05	1·952	−0·119	−0·769	−1·544
1·13	1·785	0·591	−0·236	−0·712	1·10	1·893	−0·512	−1·125	−1·894

Slots Sealed

0·40	1·483	1·571	1·015	0·488	0·40	1·425	1·383	0·900	0·343
0·51	1·556	1·567	1·035	0·432	0·50	1·469	1·375	0·877	0·303
0·61	1·610	1·527	0·939	0·351	0·60	1·516	1·328	0·813	0·221
0·71	1·699	1·595	0·979	0·355	0·70	1·593	1·309	0·767	0·146
0·81	1·820	1·565	0·877	0·237	0·80	1·692	1·200	0·624	−0·035
					0·85	1·796	1·143	0·531	−0·168

TABLE 10

Calculated Lift Derivatives for Delta Wing, $A = 2{\cdot}64$

25 in. × 20 in. Perforated Tunnel.

M	l_θ		$l_{\dot\theta_1}$		$l_{\dot\theta_2}$	$l_{\dot\theta_3}$	
	1 in. gap	$2\frac{1}{2}$ in. gap	1 in. gap	$2\frac{1}{2}$ in. gap	1 in. gap	1 in. gap	$2\frac{1}{2}$ in. gap
0·40	1·427	1·311	1·520	1·511	1·043	0·495	0·560
0·50	1·451	1·393	1·535	1·504	1·072	0·467	0·493
0·60	1·493	1·419	1·429	1·487	0·939	0·345	0·458
0·70	1·558	1·466	1·388	1·451	0·877	0·259	0·388
0·80	1·580	1·539	1·217	1·447	0·697	0·072	0·331
0·85	1·667	1·585	1·197	1·528	0·651	−0·009	0·378
0·90	1·772	1·643	1·205	1·623	0·618	−0·069	0·432
0·95	1·991	1·817	0·903	1·512	0·189	−0·448	0·194
1·00	1·915	1·875	−0·356	0·263	−1·139	−1·591	−1·097
1·05	1·900		−0·261		−0·890	−1·643	
1·10	1·900		−0·538		−1·186	−1·897	
1·20	1·700		−0·099		−0·697	−1·303	
1·30	1·580		0·082		−0·476	−1·035	
1·40	1·443		0·026		−0·313	−1·167	

Perforations Sealed.

M	l_θ	$l_{\dot\theta_1}$	$l_{\dot\theta_2}$	$l_{\dot\theta_3}$
0·40	1·473	1·452	0·957	0·389
0·50	1·501	1·425	0·914	0·349
0·60	1·556	1·416	0·891	0·294
0·70	1·599	1·381	0·847	0·222
0·80	1·692	1·327	0·764	0·099
0·85	1·726	1·337	0·803	0·044

TABLE 11

Calculated Lift Derivatives for Delta Wing, $A = 2{\cdot}64$

36 in. × 14 in. Slotted Tunnel.

M	l_θ	$l_{\dot{\theta}_1}$	$l_{\dot{\theta}_2}$	$l_{\dot{\theta}_3}$
0·40	1·314	1·275	0·902	0·316
0·50	1·352	1·257	0·837	0·270
0·60	1·360	1·252	0·872	0·259
0·70	1·431	1·199	0·729	0·155
0·80	1·485	1·149	0·641	0·065
0·85	1·524	1·165	0·703	0·052
0·90	1·563	1·115	0·660	−0·026
0·95	1·652	1·001	0·542	−0·205
1·00	1·791	0·055	−0·470	−1·253
1·05	1·802	−0·256	−0·975	−1·572
1·10	1·802	−0·209	−0·963	−1·524

Slots Sealed

0·40	1·313	1·264	0·887	0·306
0·50	1·365	1·270	0·870	0·274
0·60	1·422	1·257	0·838	0·220
0·70	1·476	1·209	0·789	0·132
0·80	1·539	1·181	0·736	0·058
0·85	1·626	1·045	0·520	−0·142

TABLE 12

Corrected Derivatives for Delta Wing A = 2·64 9½ in. × 9½ in. Tunnel

Slotted Tunnel

M	$-m_{\theta_1}$	$-m_{\theta_2}$	m_{θ_3}	$-m_{\dot{\theta}_1}$	$-m_{\dot{\theta}_2}$	$-m_{\dot{\theta}_3}$	l_θ	$l_{\dot{\theta}_1}$	$l_{\dot{\theta}_2}$	$l_{\dot{\theta}_3}$
0·41	0·542	0·005	0·592	1·034	0·365	0·113	1·560	1·846	1·443	0·703
0·51	0·571	0·011	0·589	1·048	0·378	0·116	1·597	1·854	1·414	0·685
0·61	0·608	0·021	0·616	1·047	0·426	0·172	1·683	1·808	1·207	0·571
0·66	0·621	0·029	0·626	1·122	0·447	0·202	1·718	1·803	1·304	0·580
0·82	0·664	0·046	0·651	1·299	0·585	0·430	1·823	1·819	1·494	0·486
0·87	0·723	0·065	0·670	1·322	0·643	0·609	1·938	1·700	1·495	0·266

Slots Sealed

0·40	0·476	0·012	0·511	0·879	0·383	0·168	1·348	1·495	0·989	0·499
0·51	0·503	0·007	0·527	0·886	0·373	0·189	1·406	1·492	1·008	0·454
0·61	0·509	−0·001	0·550	0·898	0·411	0·240	1·445	1·460	0·933	0·394
0·66	0·518	−0·004	0·562	0·928	0·434	0·262	1·481	1·486	0·964	0·395
0·81	0·559	−0·015	0·605	1·090	0·594	0·435	1·584	1·511	0·916	0·342
0·87	0·575	−0·028	0·624	1·169	0·700	0·600	1·636	1·498	1·023	0·302

TABLE 13

Corrected Derivatives for Delta Wing A = 2·64 9½ in. × 9½ in. Tunnel with ½ in. Step

Slotted Tunnel

M	$-m_{\theta_1}$	$-m_{\theta_2}$	m_{θ_3}	$-m_{\dot{\theta}_1}$	$-m_{\dot{\theta}_2}$	$-m_{\dot{\theta}_3}$	l_θ	$l_{\dot{\theta}_1}$	$l_{\dot{\theta}_2}$	$l_{\dot{\theta}_3}$
0·42	0·476	0·033	0·475	0·801	0·314	0·142	1·317	1·374	0·925	0·415
0·53	0·489	0·033	0·481	0·808	0·329	0·160	1·343	1·356	0·905	0·398
0·63	0·514	0·039	0·493	0·923	0·353	0·174	1·397	1·564	1·043	0·456
0·74	0·542	0·049	0·509	1·001	0·438	0·216	1·461	1·578	1·082	0·517
0·85	0·592	0·070	0·537	1·088	0·510	0·396	1·568	1·539	0·953	0·278
0·90	0·631	0·087	0·558	1·087	0·552	0·514	1·656	1·391	0·781	0·065

TABLE 14

Corrected Derivatives for Delta Wing A = 2·64. 18 in. × 14 in. Tunnel

Slotted Tunnel

M	$-m_{\theta_1}$	$-m_{\theta_2}$	m_{θ_3}	$-m_{\dot{\theta}_1}$	$-m_{\dot{\theta}_2}$	$-m_{\dot{\theta}_3}$	l_θ	$l_{\dot{\theta}_1}$	$l_{\dot{\theta}_2}$	$l_{\dot{\theta}_3}$
0·40	0·532	0·028	0·541	0·814	0·334	0·205	1·470	1·371	0·874	0·300
0·50	0·528	0·025	0·543	0·820	0·354	0·237	1·467	1·336	0·842	0·268
0·60	0·547	0·027	0·561	0·835	0·381	0·293	1·518	1·298	0·785	0·193
0·66	0·548	0·024	0·570	0·850	0·411	0·341	1·539	1·267	0·744	0·154
0·80	0·604	0·035	0·604	0·896	0·510	0·537	1·656	1·089	0·531	−0·115
0·87	0·628	0·035	0·631	0·964	0·617	0·711	1·738	0·939	0·379	−0·300

Slots Sealed

0·40	0·505	0·026	0·517	0·823	0·342	0·194	1·400	1·383	0·908	0·359
0·50	0·511	0·018	0·541	0·826	0·351	0·218	1·442	1·377	0·887	0·322
0·60	0·525	0·015	0·561	0·843	0·381	0·280	1·487	1·334	0·828	0·246
0·66	0·536	0·017	0·570	0·865	0·410	0·315	1·537	1·336	0·802	0·228
0·80	0·593	0·026	0·615	0·965	0·539	0·523	1·653	1·225	0·661	0·016
0·87	0·639	0·027	0·668	1·066	0·666	0·723	1·803	1·163	0·639	−0·133

TABLE 15

Corrected Derivatives for Delta Wing A = 2·64. 25 in. × 20 in. Tunnel

Perforated Tunnel

M	$-m_{\theta_1}$	m_{θ_2}*	m_{θ_3}	$-m_{\dot{\theta}_1}$	$-m_{\dot{\theta}_2}$*	$-m_{\dot{\theta}_3}$	l_θ	$l_{\dot{\theta}_1}$	$l_{\dot{\theta}_2}$*	$l_{\dot{\theta}_3}$
0·40	0·468	0·001	0·500	0·836	0·338	0·168	1·334	1·419	0·944	0·456
0·50	0·502	0·000	0·527	0·851	0·356	0·221	1·419	1·391	0·953	0·364
0·60	0·511	0·000	0·538	0·865	0·386	0·268	1·447	1·357	0·798	0·312
0·66	0·523	0·001	0·547	0·878	0·409	0·315	1·476	1·321	0·719	0·248
0·80	0·562	0·004	0·579	0·941	0·500	0·466	1·573	1·229	0·460	0·093
0·87	0·586	−0·001	0·607	1·053	0·600	0·558	1·640	1·272	0·286	0·087

Perforations Sealed

0·40	0·514	−0·008	0·521	0·840	0·339	0·180	1·428	1·433	0·959	0·396
0·50	0·521	−0·005	0·535	0·854	0·367	0·218	1·455	1·413	0·917	0·357
0·60	0·536	−0·004	0·559	0·877	0·391	0·268	1·511	1·402	0·896	0·305
0·66	0·543	−0·004	0·569	0·898	0·414	0·307	1·532	1·380	0·877	0·263
0·80	0·583	−0·005	0·604	0·983	0·520	0·472	1·636	1·309	0·778	0·121
0·87	0·598	−0·001	0·631	1·111	0·613	0·634	1·685	1·275	0·834	0·044

*1 in. gap

TABLE 16

Corrected Derivatives for Delta Wing A = 2·64. 36 in. × 14 in. Tunnel

Slotted Tunnel

M	$-m_{\theta_1}$	$-m_{\theta_2}$	m_{θ_3}	$-m_{\dot{\theta}_1}$	$-m_{\dot{\theta}_2}$	$-m_{\dot{\theta}_3}$	l_θ	$l_{\dot{\theta}_1}$	$l_{\dot{\theta}_2}$	$l_{\dot{\theta}_3}$
0·40	0·490	0·003	0·476	0·744	0·295	0·207	1·324	1·209	0·835	0·245
0·50	0·500	0·006	0·492	0·745	0·318	0·241	1·362	1·182	0·759	0·189
0·60	0·492	0·009	0·508	0·770	0·336	0·286	1·370	1·168	0·787	0·171
0·66	0·519	0·009	0·518	0·765	0·362	0·321	1·420	1·129	0·679	0·099
0·80	0·545	0·013	0·548	0·799	0·445	0·458	1·498	1·013	0·501	−0·078
0·87	0·562	0·010	0·573	0·896	0·528	0·599	1·553	0·977	0·518	−0·145

Slots Sealed

0·40	0·467	0·003	0·482	0·778	0·303	0·181	1·300	1·302	0·927	0·350
0·50	0·482	0·017	0·504	0·800	0·324	0·211	1·351	1·314	0·917	0·326
0·60	0·511	0·015	0·516	0·833	0·355	0·255	1·406	1·310	0·894	0·281
0·66	0·516	0·017	0·528	0·832	0·375	0·319	1·435	1·301	0·870	0·242
0·80	0·538	0·012	0·573	0·947	0·482	0·440	1·520	1·270	0·828	0·157
0·87	0·572	0·011	0·612	1·005	0·675	0·689	1·618	1·118	0·557	−0·051

TABLE 17

Corrected Derivatives for Delta Wing

$A = 2{\cdot}64$ in the Transonic Range Using the Method Suggested in the Text. $x_0 = 1{\cdot}04\bar{c}$.

M	$9\frac{1}{2}$ in. × $9\frac{1}{2}$ in. Slotted Tunnel			
	l_θ	$l_{\dot{\theta}}$	m_θ	$-m_{\dot{\theta}}$
0·98	1·93	0·19	0·67	1·19
1·03	1·96	−0·57	0·62	1·32
1·08	2·10	−1·62	0·59	1·40
1·10	2·11	−1·90	0·57	1·42
$9\frac{1}{2}$ in. × $9\frac{1}{2}$ in. Slotted Tunnel with $\frac{1}{2}$ in. step				
0·90	1·48	0·24	0·56	0·43
0·96	1·53	0·29	0·59	0·64
1·02	1·62	0·11	0·56	0·87
1·07	1·73	−0·14	0·58	1·19
1·13	2·00	−1·27	0·55	1·18
18 in. × 14 in. Slotted Tunnel				
0·95	1·93	−0·86	0·58	1·15
1·00	1·99	−2·28	0·51	1·01
1·05	1·99	−2·21	0·46	0·90
1·10	1·96	−2·52	0·43	0·91
25 in. × 20 in. Perforated Tunnel, $2\frac{1}{2}$ in. gap				
0·95	1·86	−0·23	0·58	0·95
1·00	1·92	−1·57	0·51	0·90
1·10	1·90*	−2·33*	0·44*	1·00*
36 in. × 14 in. Slotted Tunnel				
0·95	1·66	−0·43	0·56	0·99
1·00	1·81	−1·52	0·51	0·96
1·05	1·82	−1·85	0·45	0·91
1·10	1·82	−2·18	0·42	0·75

*Values for $M = 1{\cdot}10$ are estimated

TABLE 18

Measured Derivatives for Tapered Wing, A = 4·33

36 in. × 14 in. Slotted Tunnel.

M	l_{θ_2}	$-l_{\dot{\theta}_2}$	$-m_{\theta_1}$	m_{θ_2}	m_{θ_3}	$-m_{\dot{\theta}_1}$	$-m_{\dot{\theta}_2}$	$-m_{\dot{\theta}_3}$
0·60	2·255	0·796	0·256	0·604	1·452	0·552	0·759	1·711
0·70	2·408	1·256	0·270	0·648	1·555	0·602	1·006	2·003
0·79	2·610	1·814	0·295	0·696	1·676	0·685	1·312	2·652
0·84	2·732	2·374	0·365	0·695	1·728	0·722	1·563	3·179
0·87			0·436					
0·89	2·973	3·893	0·509	0·613	1·706	0·359	1·611	3·626
0·92			0·434					
0·94	2·447	2·686	0·315	0·645	1·581	0·598	1·580	3·207
0·99	2·580	2·743	0·428	0·581	1·655	0·865	1·904	3·543
1·04	2·586	3·839	0·447	0·571	1·542	0·799	2·353	4·410
1·09	2·536	3·625	0·410	0·571	1·530	1·223	2·985	5·074

Slots Sealed

0·60	2·243	0·737	0·253	0·622	1·510	0·550	0·751	1·666
0·71	2·427	1·230	0·279	0·659	1·593	0·591	0·999	2·161
0·81	2·659	2·170	0·332	0·709	1·744	0·663	1·464	3·034
0·87	2·936	3·687	0·496	0·667	1·799	0·440	1·786	3·957

25 in. × 20 in. Slotted Tunnel

M	Slotted		Slots Sealed	
	m_{θ_2}	$-m_{\dot{\theta}_2}$	m_{θ_2}	$-m_{\dot{\theta}_2}$
0·60	0·587	0·417	0·627	0·635
0·70	0·607	0·490	0·666	0·843
0·80	0·643	0·663	0·720	1·308
0·85	0·635	0·809	0·655	1·588
0·90	0·554	0·876		
0·95	0·606	1·020		
1·00	0·570	1·516		
1·05	0·571	2·026		
1·10	0·616	3·989		

TABLE 19

Measured Derivatives for Tapered Wing, $A = 4{\cdot}33$

25 in. × 20 in. Perforated Tunnel

M	l_{θ_2}	$-l_{\dot{\theta}_2}$	$-m_{\theta_1}$	m_{θ_2}	m_{θ_3}	$-m_{\dot{\theta}_1}$	$-m_{\dot{\theta}_2}$	$-m_{\dot{\theta}_3}$
0·40	1·963	−0·215	0·221	0·539	1·305	0·558	0·310	0·590
0·50	2·022	−0·119	0·228	0·555	1·347	0·605	0·339	0·621
0·60	2·013	−0·176	0·235	0·574	1·395	0·660	0·402	0·791
0·70	2·078	−0·100	0·251	0·597	1·459	0·713	0·551	1·161
0·80	2·307	0·520	0·278	0·626	1·551	0·809	0·856	1·842
0·85	2·463	0·657	0·338	0·616	1·594	0·850	1·074	2·276
0·90	2·423	1·053	0·448	0·543	1·557*	0·730	1·215	2·416*
0·95					1·468			2·445
1·00	2·245	1·310	0·314	0·581	1·511	1·195	1·987	3·110
1·10	2·495	3·975	0·424	0·590	1·697	0·606	2·885	6·234
1·20	2·740	6·385	0·666	0·438	1·383	1·059	1·277	3·192
1·30	2·378	3·603	0·666	0·083	1·128	0·617	0·144	2·278
1·40	2·056	2·369	0·620	0·045	0·928	0·373	0·078	1·553

*$M = 0{\cdot}885$

Perforations Sealed

0·40	2·013	0·061	0·241	0·579	1·413	0·522	0·417	0·926
0·50	2·099	0·178	0·251	0·599	1·480	0·546	0·490	1·122
0·60	2·178	0·318	0·265	0·629	1·538	0·590	0·616	1·353
0·70	2·328	0·482	0·288	0·665	1·635	0·654	0·801	1·726
0·80	2·515	1·041	0·346	0·697	1·778	0·740	1·151	2·503
0·85	2·740	1·885	0·478	0·653	1·786	0·659	1·406	3·182

M	8/63 Perforated		4/9 Perforated	
	m_{θ_3}	$-m_{\dot{\theta}_3}$	m_{θ_3}	$-m_{\dot{\theta}_3}$
0·40	1·368	0·902	1·351	0·683
0·50	1·443	1·077	1·389	0·764
0·60	1·502	1·269	1·460	0·926
0·70	1·581	1·555	1·525	1·231
0·80	1·686	2·138	1·618	1·862
0·85	1·716	2·653	1·647	2·349
0·90			1·528	2·399

TABLE 20

Calculated Lift Derivatives for Tapered Wing, A = 4·33

25 in. × 20 in. Perforated Tunnel

M	l_θ	$l_{\dot{\theta}_1}$	$l_{\dot{\theta}_2}$	$-l_{\dot{\theta}_3}$
0·40	1·932	1·167	0·502	0·170
0·50	1·994	1·229	0·540	0·159
0·60	2·064	1·227	0·414	0·411
0·70	2·165	1·007	0·037	0·948
0·80	2·316	0·507	−0·672	1·871
0·85	2·446	0·049	−1·177	2·427
0·90	2·538	−0·685	−1·580	2·498
1·00	2·310	−1·424	−1·826	2·262
1·10	2·685	−5·180	−6·489	7·890
1·20	2·594	−5·477	−5·024	4·411
1·30	2·271	−1·844	−3·434	5·320
1·40	1·960	−1·097	−2·285	3·690

Perforations Sealed

0·40	2·094	0·845	0·075	0·710
0·50	2·191	0·741	−0·115	1·001
0·60	2·283	0·563	−0·330	1·237
0·70	2·435	0·293	−0·684	1·677
0·80	2·689	−0·344	−1·516	2·726
0·85	2·866	−1·238	−2·540	3·844

TABLE 21

Corrected Derivatives for Tapered Wing, $A = 4{\cdot}33$, $x_0 = 0{\cdot}79\bar{c}$, Ventilated Tunnels

36 in. × 14 in. Slotted Tunnel					25 in. × 20 in. Perforated Tunnel				
M	l_θ	$-l_{\dot\theta}$	m_θ	$-m_{\dot\theta}$	M	l_θ	$-l_{\dot\theta}$	m_θ	$-m_{\dot\theta}$
0·60	2·387	1·658	0·636	0·988	0·60	2·296	0·946	0·642	0·705
0·70	2·561	2·391	0·685	1·311	0·70	2·389	1·269	0·670	0·931
0·79	2·796	3·418	0·739	1·740	0·80	2·710	2·753	0·711	1·440
0·84	2·940	4·398	0·739	2·079	0·85	2·939	3·594	0·703	1·795
0·89	3·224	6·846	0·653	2·198	0·90	2·909	4·566	0·611	1·963
0·94	2·638	5·118	0·678	2·179					

Sealed Tunnels

36 in. × 14 in. Tunnel (Slots Sealed)					25 in. × 20 in. Tunnel (Perforations Sealed)				
M	l_θ	$-l_{\dot\theta}$	m_θ	$-m_{\dot\theta}$	M	l_θ	$-l_{\dot\theta}$	m_θ	$-m_{\dot\theta}$
0·60	2·083	0·200	0·583	0·604	0·60	2·021	0·140	0·592	0·568
0·71	2·238	0·497	0·615	0·798	0·70	2·145	0·251	0·624	0·735
0·81	2·427	1·059	0·657	1·161	0·80	2·292	0·677	0·652	1·046
0·87	2·654	2·012	0·617	1·401	0·85	2·473	1·330	0·610	1·271

Corrected Derivatives for Tapered Wing in the Transonic Range Using Method Suggested in Text: $x_0 = 0{\cdot}79\bar{c}$

M	36 in. × 14 in Slotted Tunnel				25 in. × 20 in. Perforated Tunnel			
	l_θ	$-l_{\dot\theta}$	m_θ	$-m_{\dot\theta}$	l_θ	$-l_{\dot\theta}$	m_θ	$-m_{\dot\theta}$
0·95	2·587	4·23	0·676	2·19	2·653	3·71	0·624	2·27
1·00	2·755	4·61	0·646	2·52	2·538	3·57	0·654	2·78
1·05	2·733	5·65	0·593	3·01	2·615	4·26	0·679	3·38
1·10	2·643	5·28	0·613	3·60	2·861	7·20	0·675	3·93

TABLE 22

Differences between Derivatives for the Tapered Wing in the 25 in. × 20 in. Perforated Tunnel and the 36 in. × 14 in. Slotted Tunnel at Transonic Speeds: $x_0 = 0{\cdot}79\bar{c}$

(a) *Measured*

M	Δl_θ	$\Delta(-l_{\dot\theta})$	Δm_θ	$\Delta(-m_{\dot\theta})$
0·95	0·110	1·40	0·090	0·19
1·00	0·355	1·53	0·029	0·01
1·05	0·270	2·04	−0·040	0·04
1·10	0·005	−0·375	−0·010	0·20

(b) *Corrected (as suggested in text)*

M	Δl_θ	$\Delta(-l_{\dot\theta})$	Δm_θ	$\Delta(-m_{\dot\theta})$
0·95	−0·066	0·52	0·052	−0·08
1·00	0·217	1·04	−0·008	−0·26
1·05	0·118	1·39	−0·086	−0·37
1·10	−0·218	−1·92	−0·062	−0·33

where

Δ = value of derivative in 36 in. × 14 in. minus value of derivative in 25 in. × 20 in.

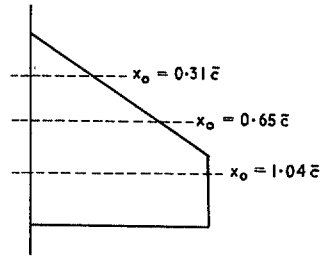

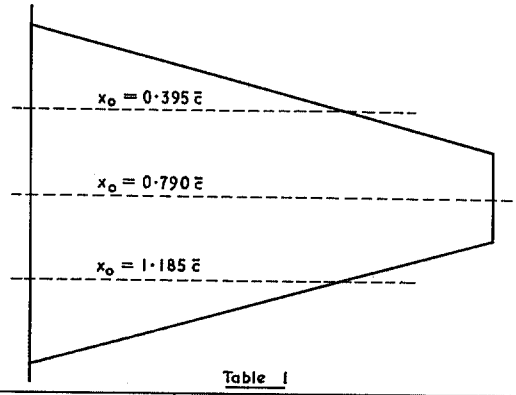

Table 1

	Delta wing	Tapered wing
Aspect ratio	2·64	4·33
Section	6% RAE 102	5% Double wedge
Taper ratio	0·389	0·266
Span (1/2 model)	3·61 in. (9·17cm)	9·59 in. (24·36 cm)
Root chord	4·00 in. (10·16 cm)	7·00 in. (17·78 cm)
Mean chord	2·75 in. (6·99cm)	4·43 in. (11·25 cm)
L.E. sweepback	33·7 deg	15·0 deg

Planforms and details of models

FIG. 1. Planforms and details of models.

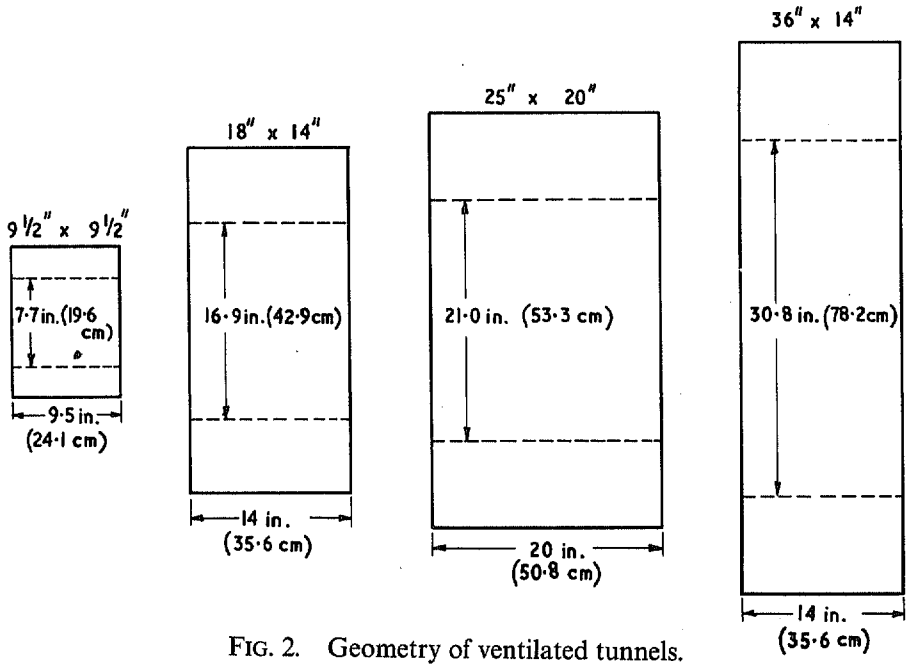

FIG. 2. Geometry of ventilated tunnels.

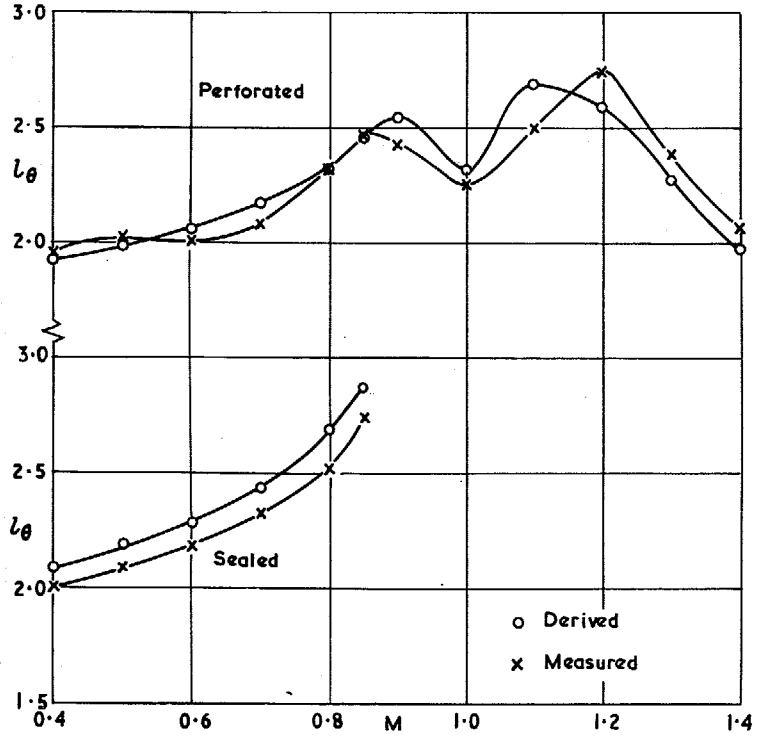

FIG. 3a. Comparison of derived and measured lift stiffness for the tapered wing in the 25 in. × 20 in. perforated tunnel. $x_0 = 0{\cdot}79\bar{c}$.

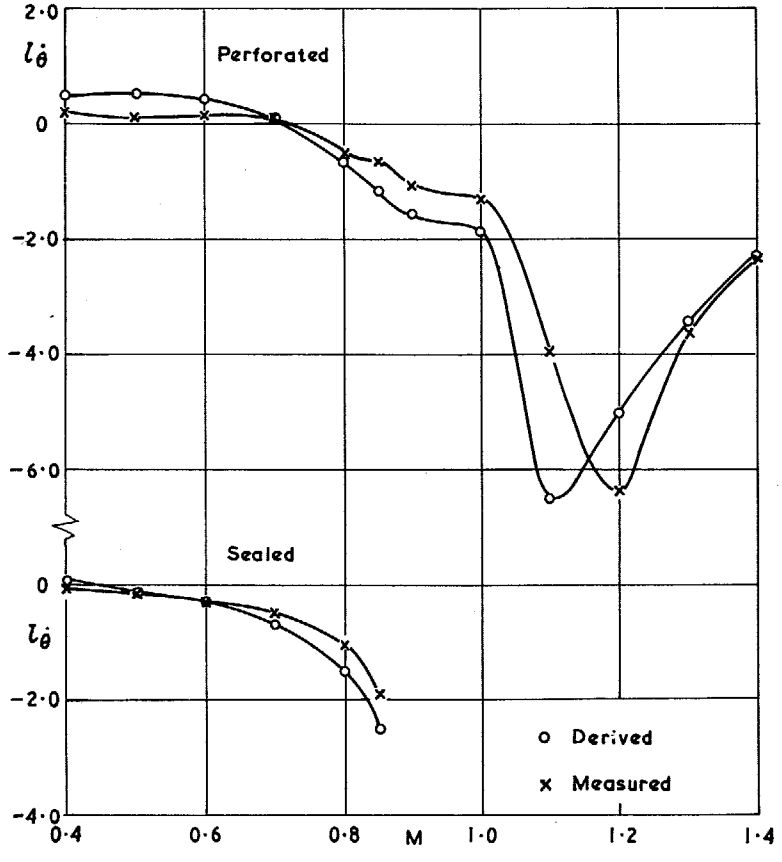

FIG. 3b. Comparison of derived and measured lift damping for the tapered wing in the 25 in. × 20 in. perforated tunnel. $x_0 = 0{\cdot}79\bar{c}$.

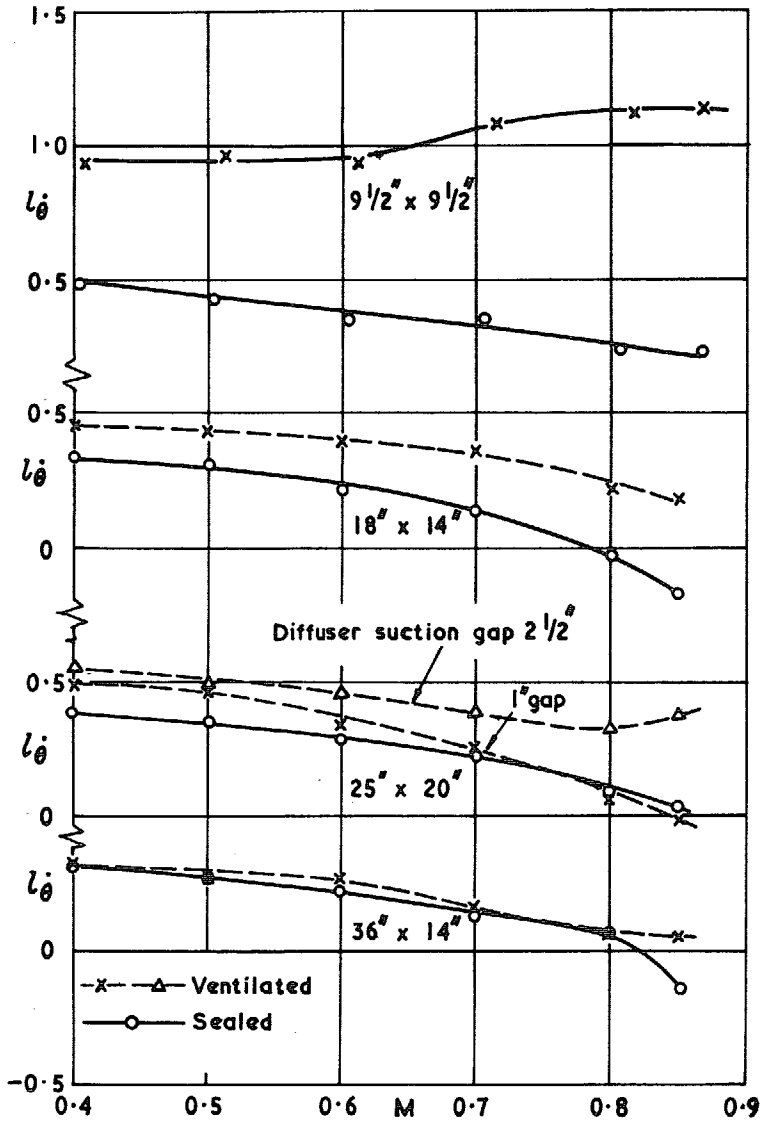

FIG. 4. Lift damping for the delta wing in ventilated and sealed tunnels at subsonic speeds. $x_0 = 1{\cdot}04\bar{c}$.

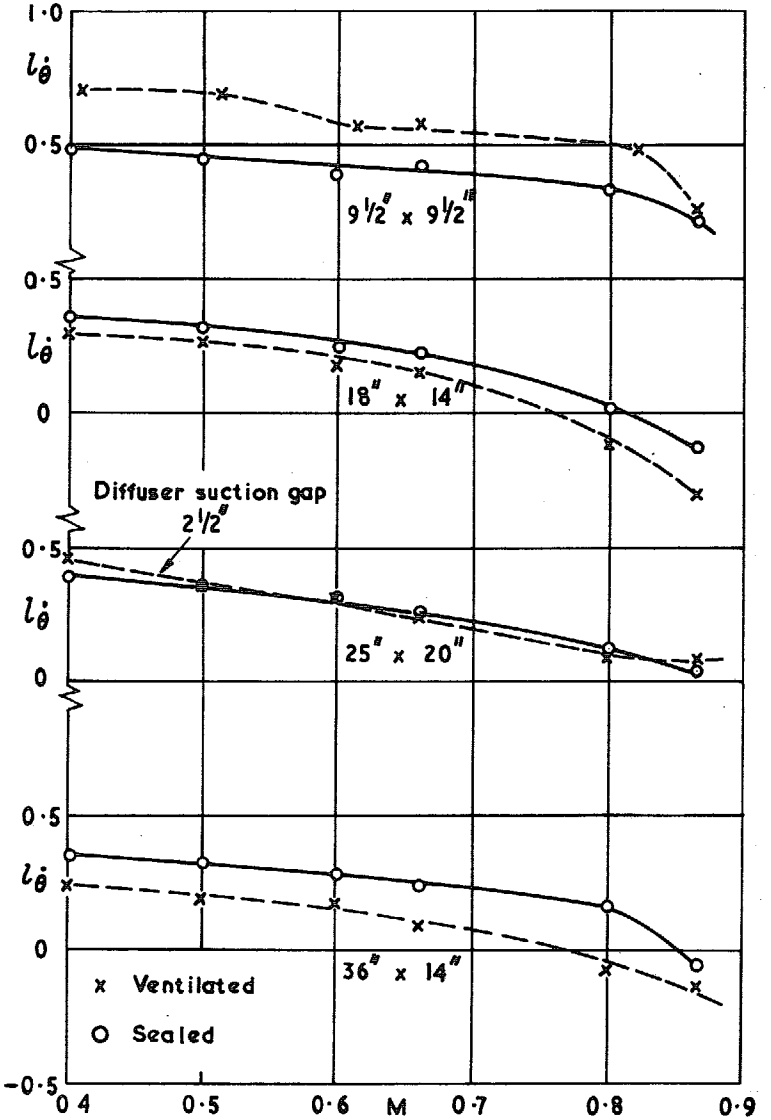

FIG. 5. Corrected lift damping for the delta wing in ventilated and sealed tunnels at subsonic speeds. $x_0 = 1{\cdot}04\bar{c}$.

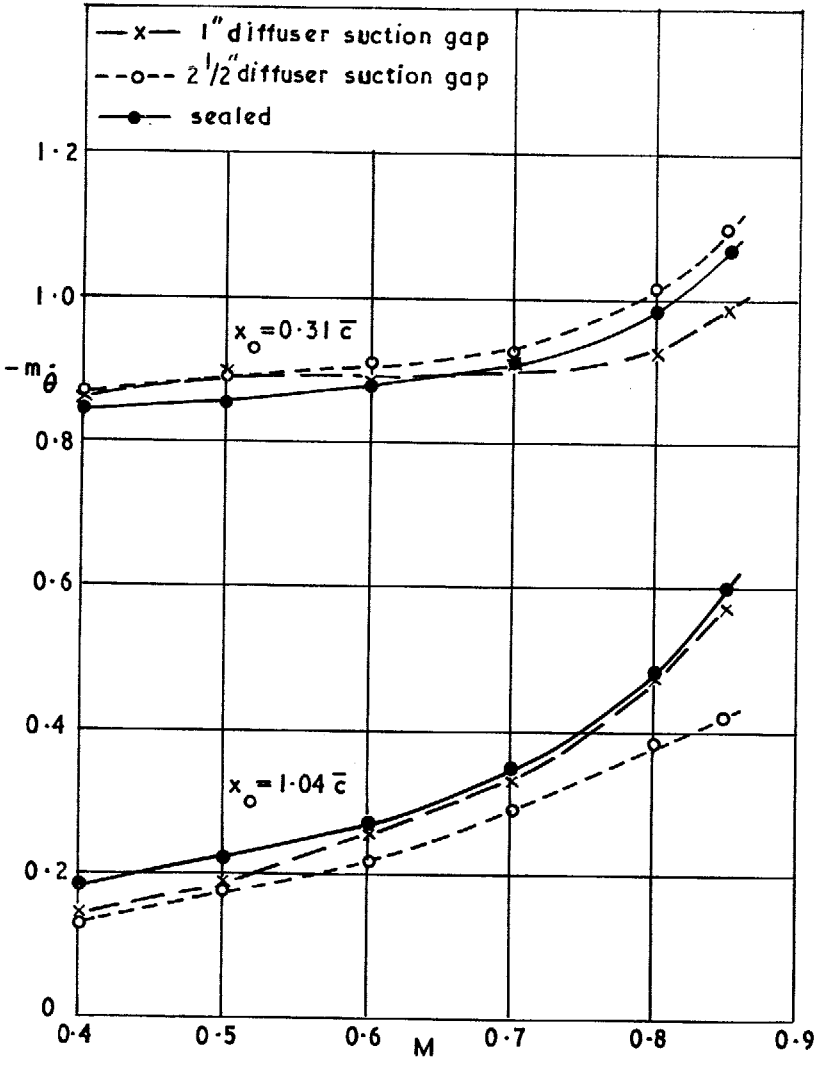

FIG. 6. Variation of derivative $m_{\dot{\theta}}$ with Mach number for the delta wing in the 25 in. × 20 in. perforated tunnel at subsonic speeds.

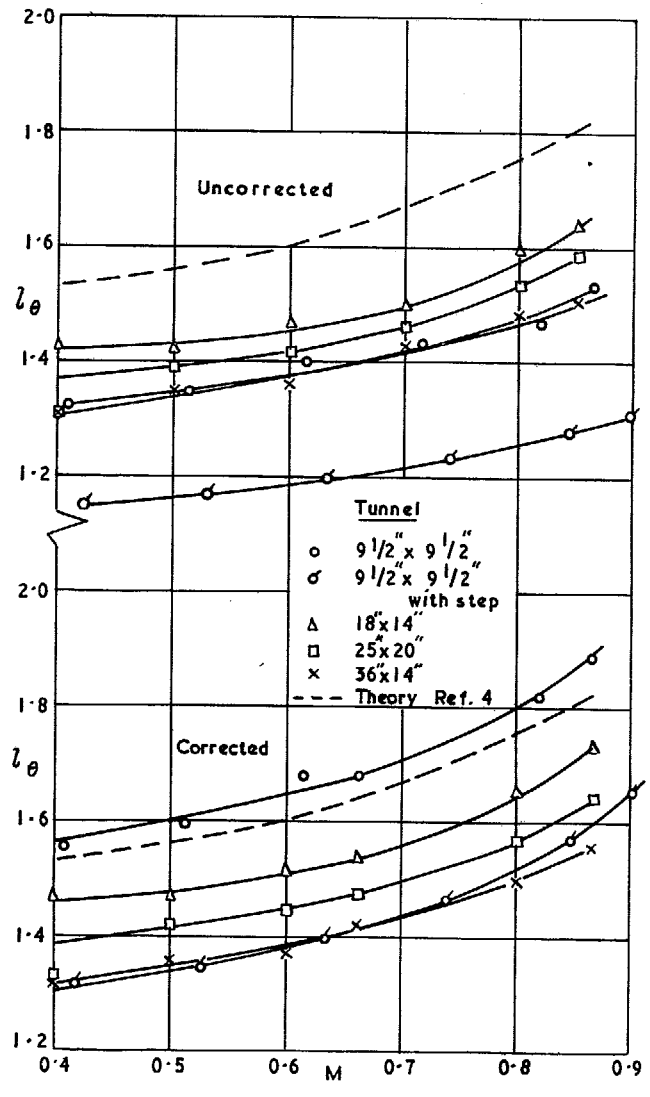

FIG. 7a. Variation of derivative l_θ with M for the delta wing in four ventilated tunnels at subsonic speeds: uncorrected and corrected.

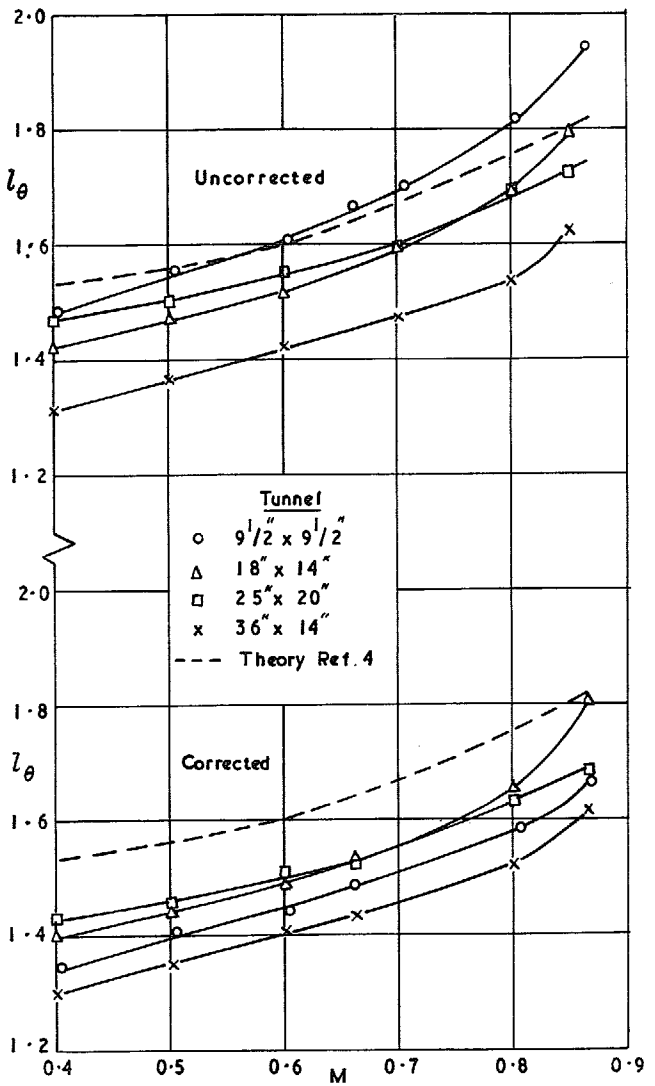

FIG. 7b. Variation of derivative l_θ with Mach number for the delta wing in four sealed tunnels: uncorrected and corrected.

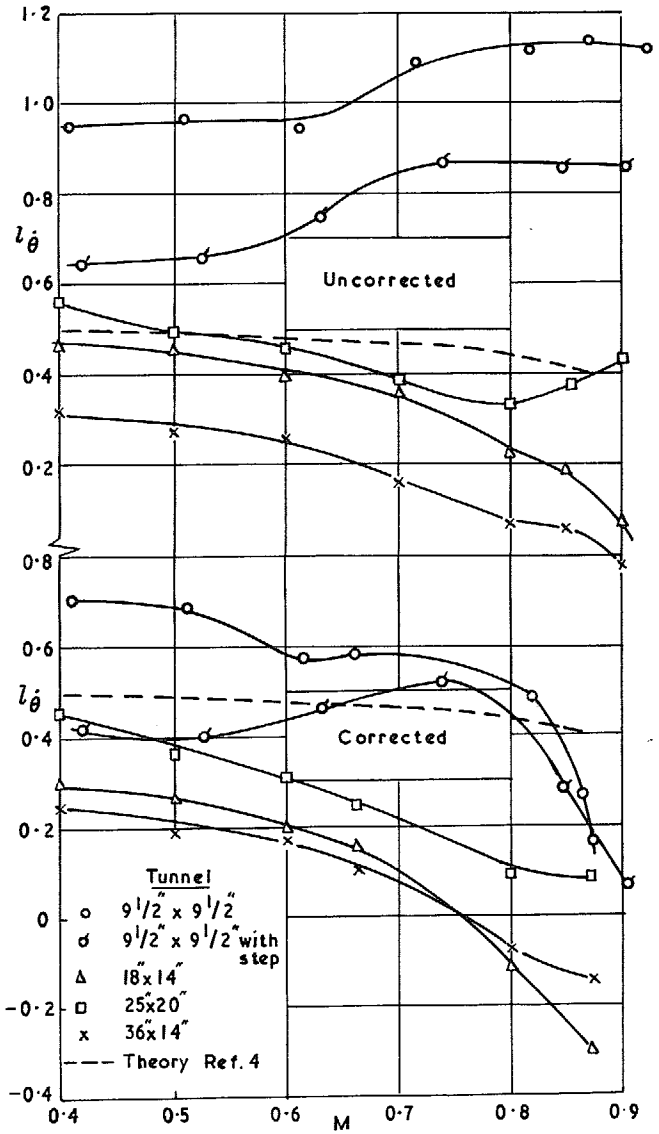

FIG. 8a. Variation of derivative $l_{\dot\theta}$ with M for the delta wing in four ventilated tunnels at subsonic speeds. $x_0 = 1{\cdot}04\bar{c}$.

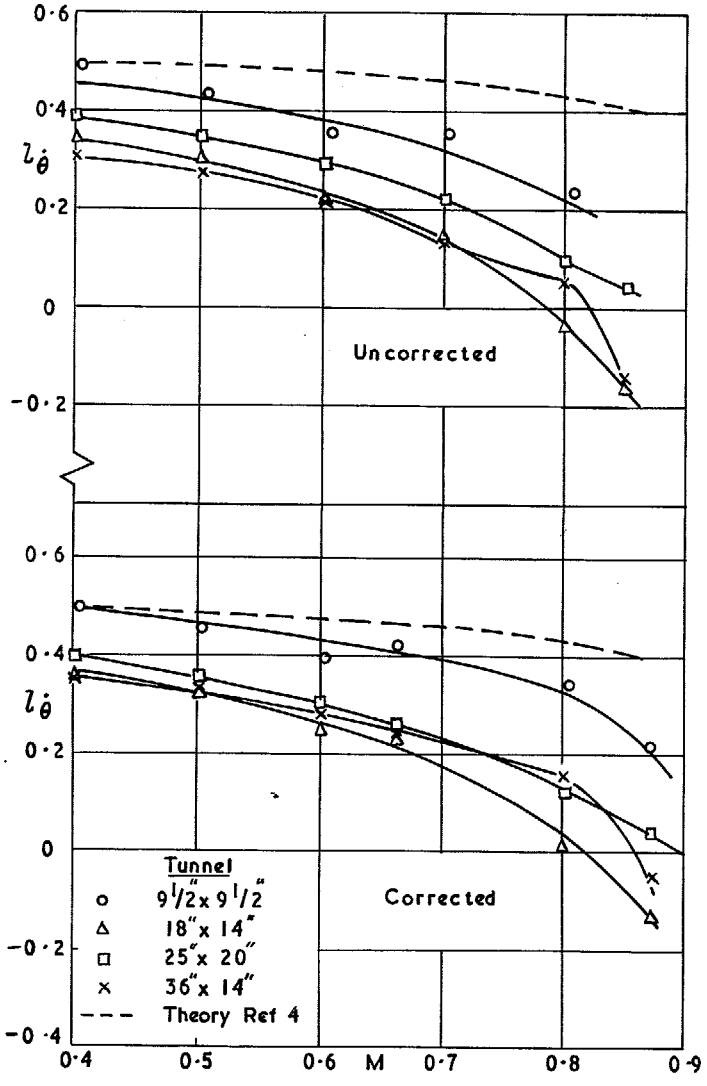

FIG. 8b. Variation of derivative $l_{\dot{\theta}}$ with M for the delta wing in four sealed tunnels. $x_0 = 1{\cdot}04\bar{c}$.

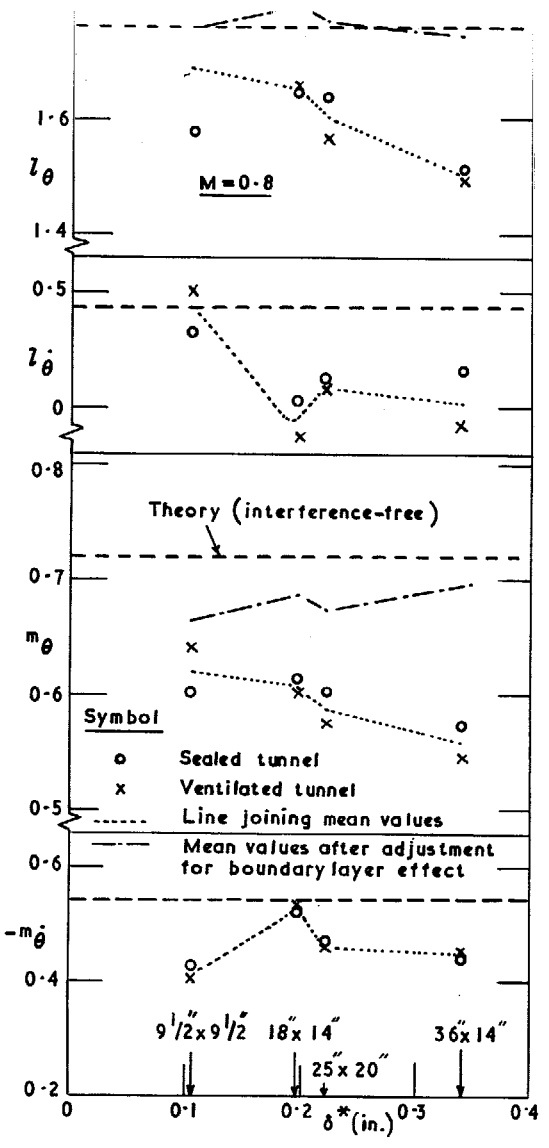

FIG. 9. Variation with boundary-layer displacement thickness of derivatives (corrected for wall interference) for the half-delta-model. $x_0 = 1{\cdot}04\bar{c}$.

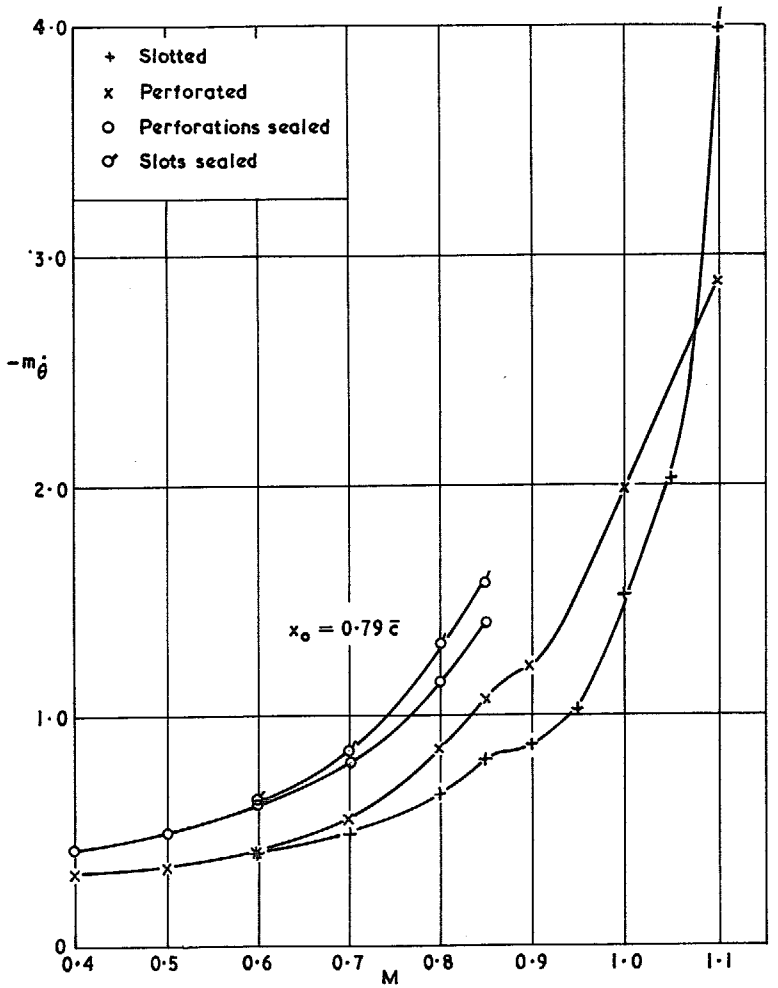

FIG. 10. Variation of derivative $m_{\dot\theta}$ with Mach number for the tapered wing in the 25 in. × 20 in. tunnel with slotted walls and with perforated walls.

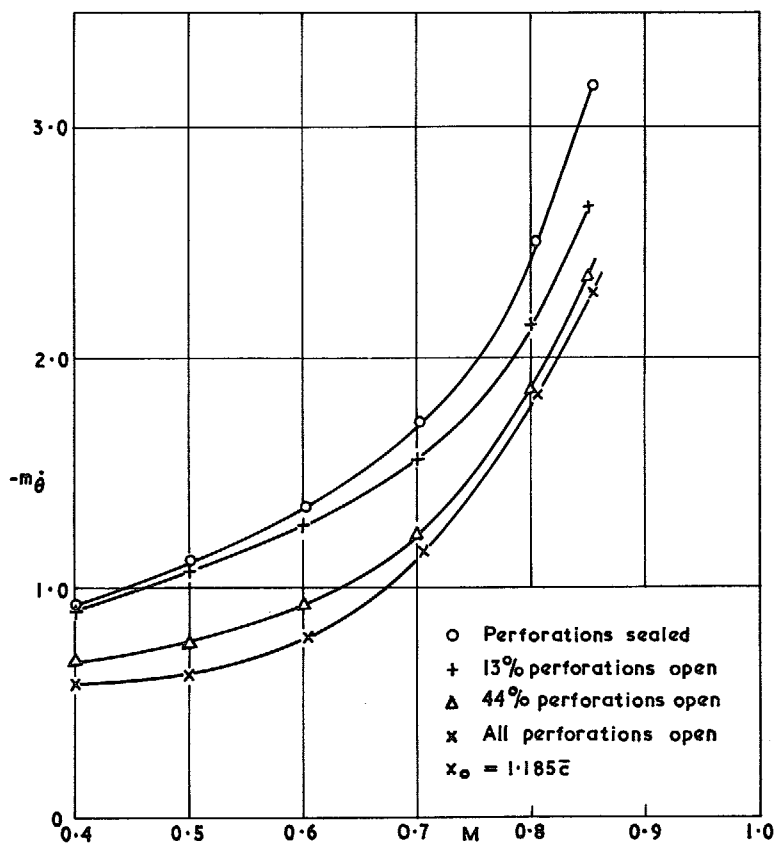

FIG 11. Variation of $m_{\dot\theta}$ with M for the tapered wing in the 25 in. × 20 in. tunnel showing the effect of reducing the open area of the perforated walls.

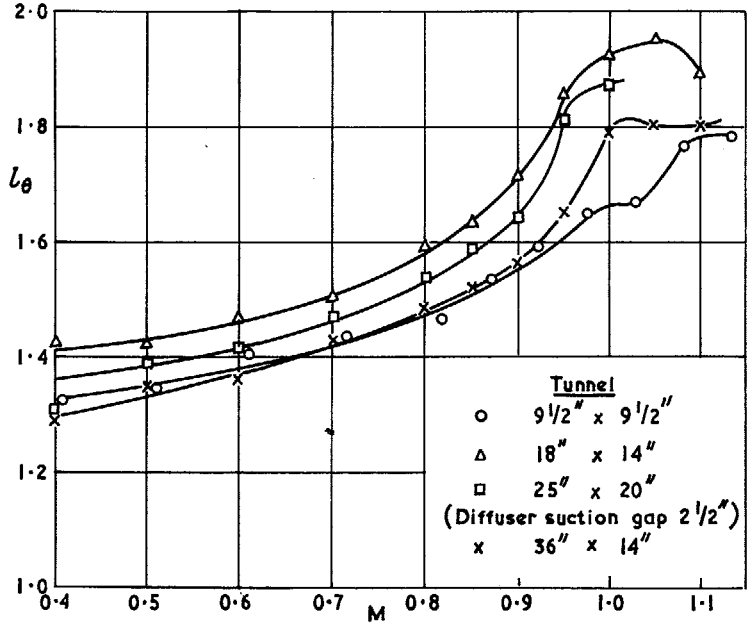

FIG. 12. Variation of derivative l_θ with Mach number for the delta wing in four ventilated tunnels including transonic speeds.

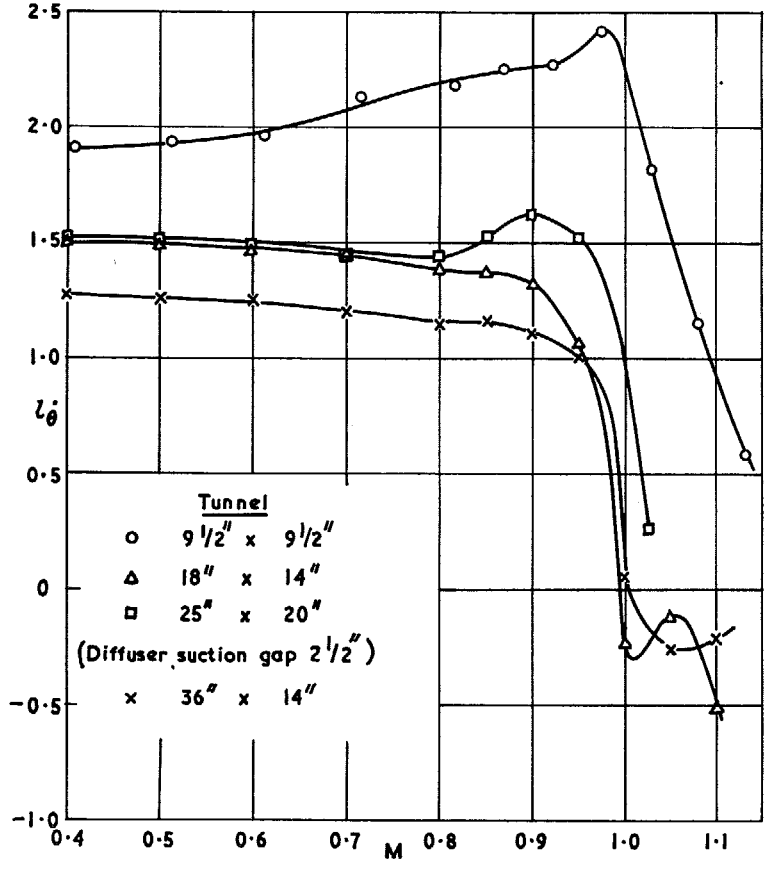

FIG. 13a. Variation of derivative $l_{\dot\theta}$ with Mach number for the delta wing in four ventilated tunnels including transonic speeds. $x_0 = 0{\cdot}31\bar{c}$.

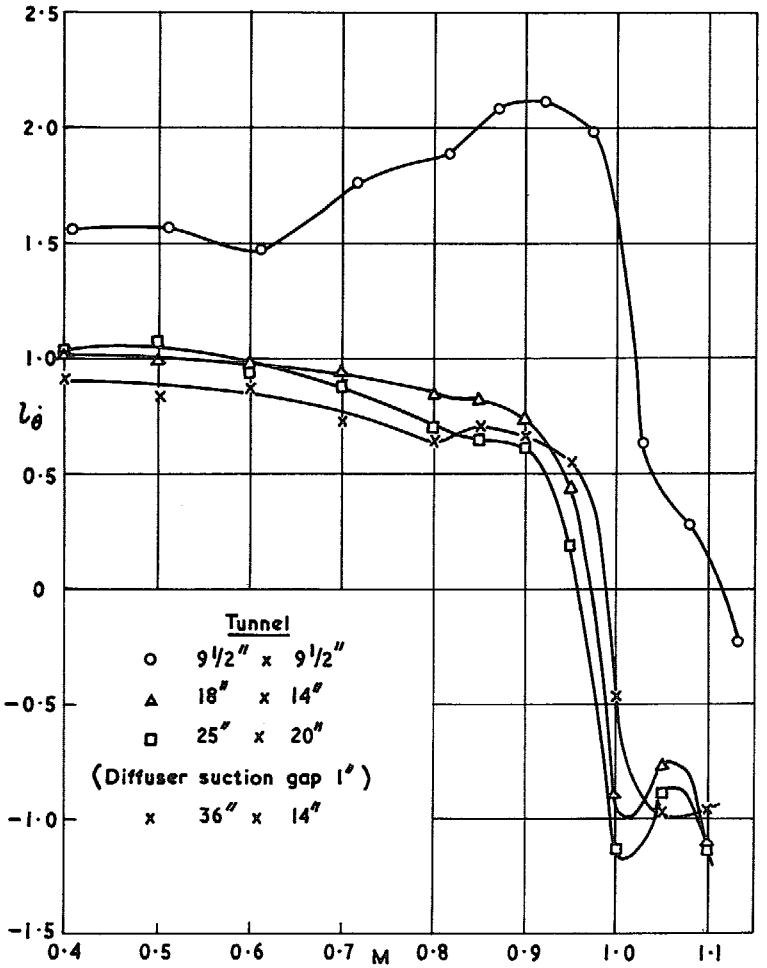

FIG. 13b. Variation of derivative $l_{\dot{\theta}}$ with Mach number for the delta wing in four ventilated tunnels including transonic speeds. $x_0 = 0{\cdot}65\bar{c}$.

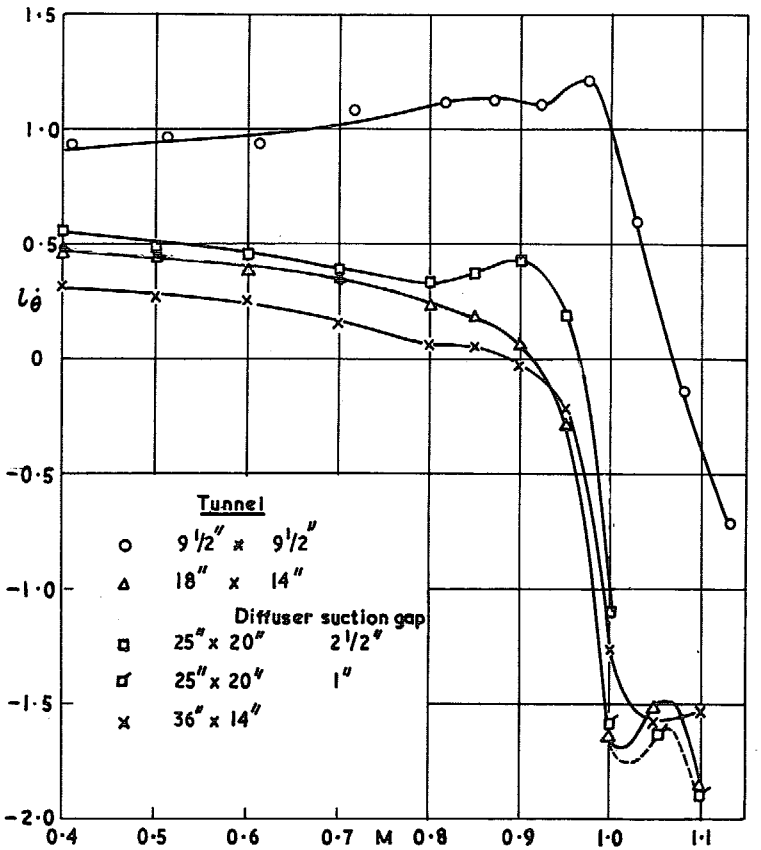

FIG. 13c. Variation of derivative $l_{\dot{\theta}}$ with Mach number for the delta wing in four ventilated tunnels including transonic speeds. $x_0 = 1{\cdot}04\bar{c}$.

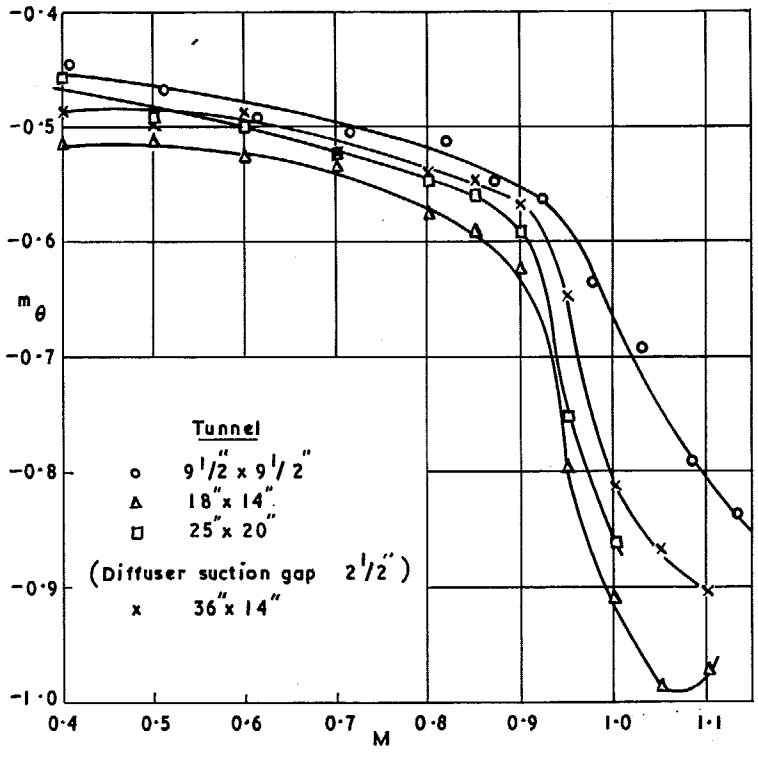

FIG. 14a. Variation of derivative m_θ with Mach number for the delta wing in four ventilated tunnels including transonic speeds. $x_0 = 0{\cdot}31\bar{c}$.

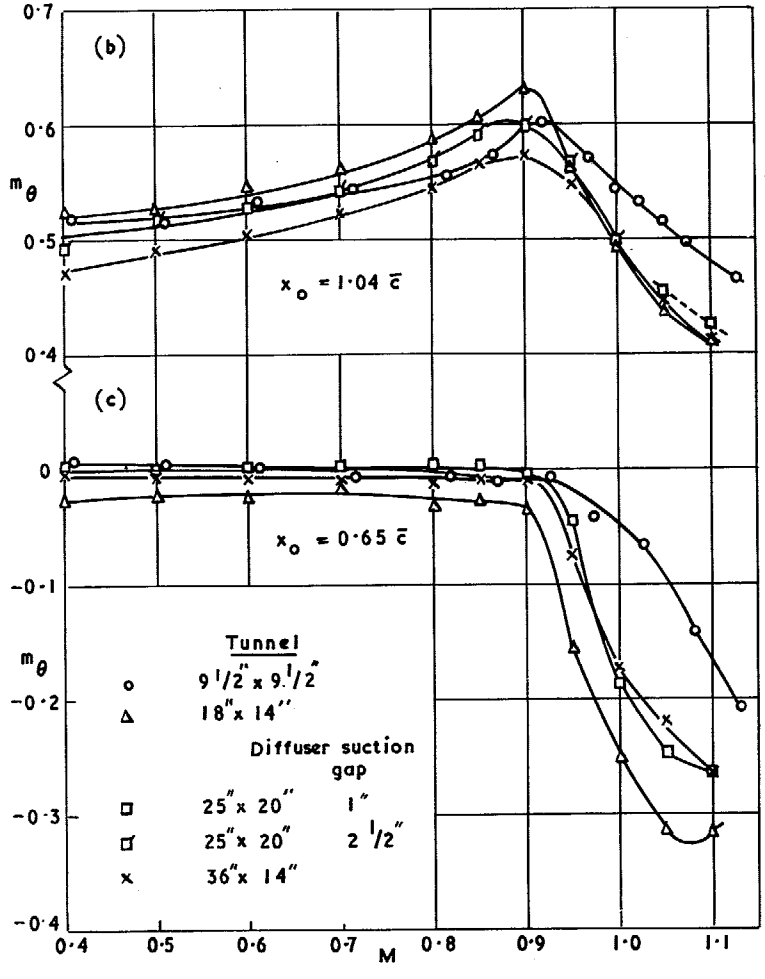

FIG. 14b and c. Variation of derivative m_θ with Mach number for the delta wing in four ventilated tunnels including transonic speeds.

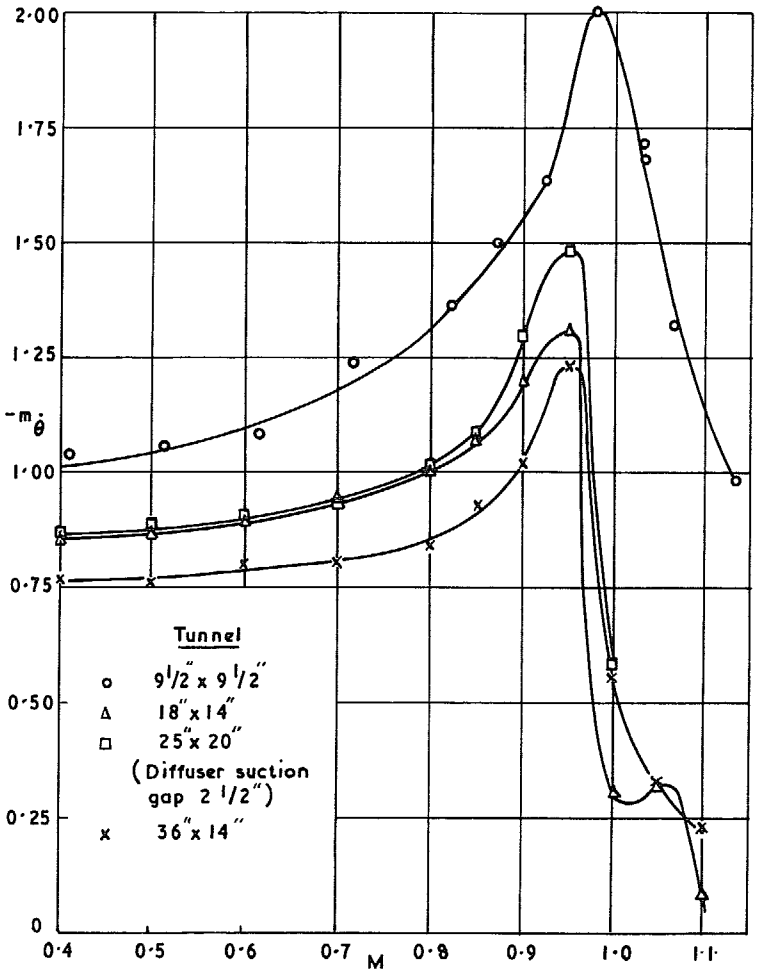

FIG. 15a. Variation of derivative $m_{\dot{\theta}}$ with Mach number for the delta wing in four ventilated tunnels including transonic speeds. $x_0 = 0{\cdot}31\bar{c}$.

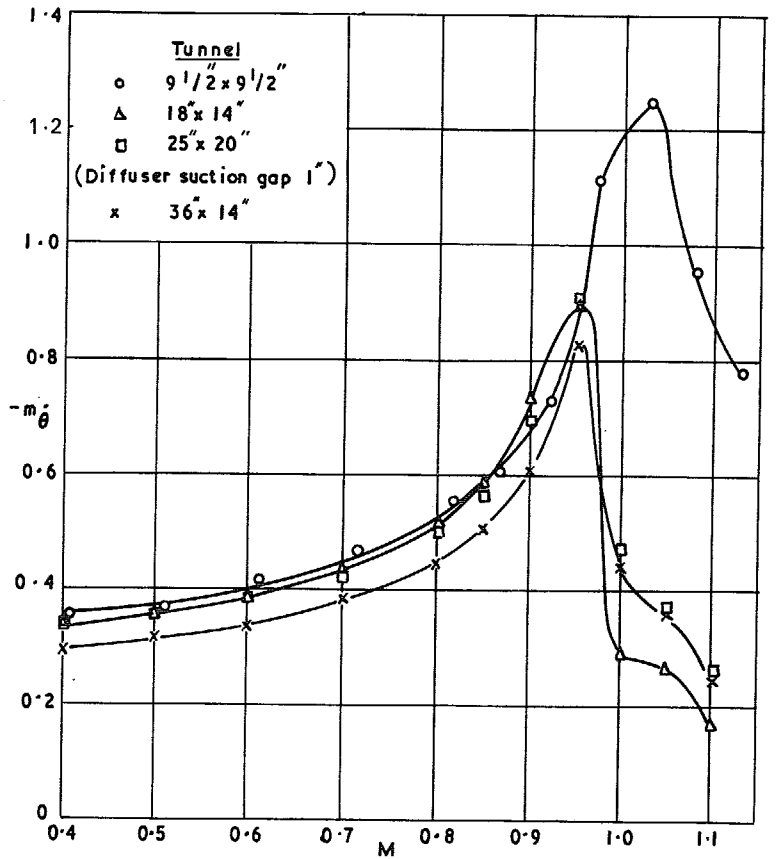

FIG. 15b. Variation of derivative $m_{\dot{\theta}}$ with Mach number for the delta wing in four ventilated tunnels including transonic speeds. $x_0 = 0{\cdot}65\bar{c}$.

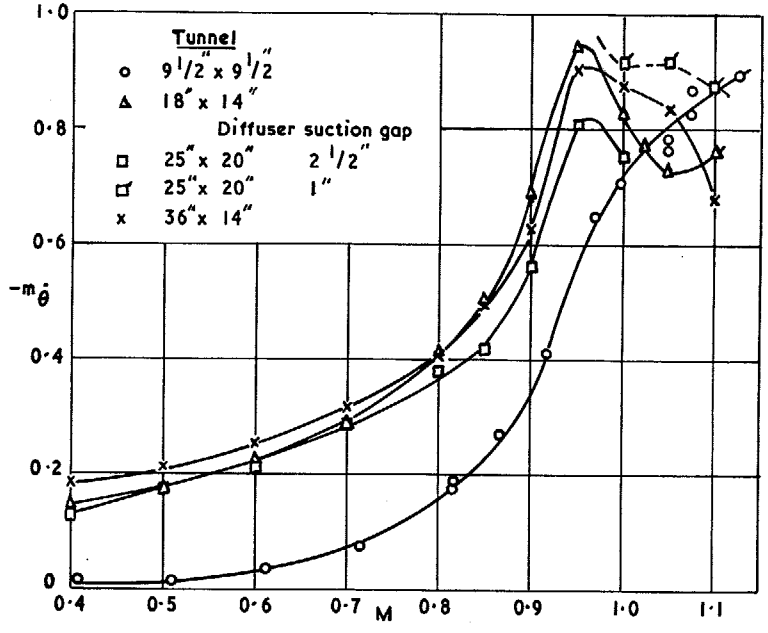

FIG. 15c. Variation of derivative $m_{\dot{\theta}}$ with Mach number for the delta wing in four ventilated tunnels including transonic speeds. $x_0 = 1{\cdot}04\bar{c}$.

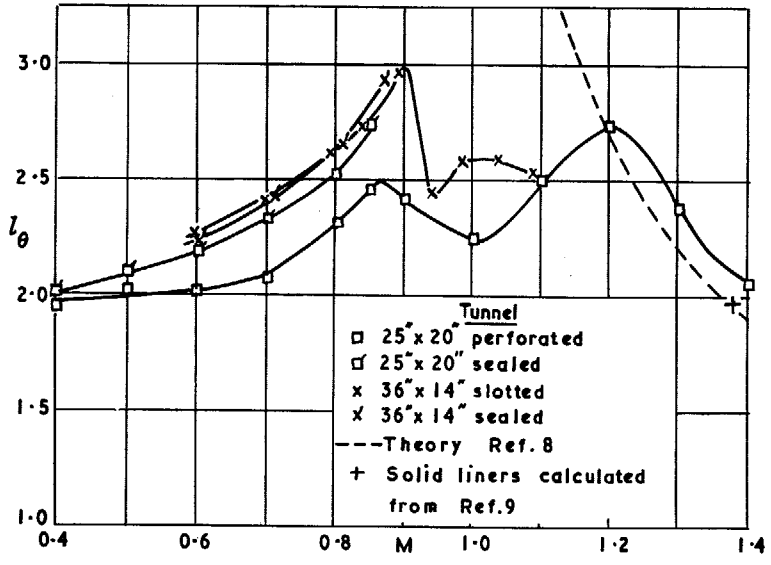

FIG. 16. Variation of derivative l_θ with Mach number for tapered wing in two ventilated tunnels including supersonic speeds.

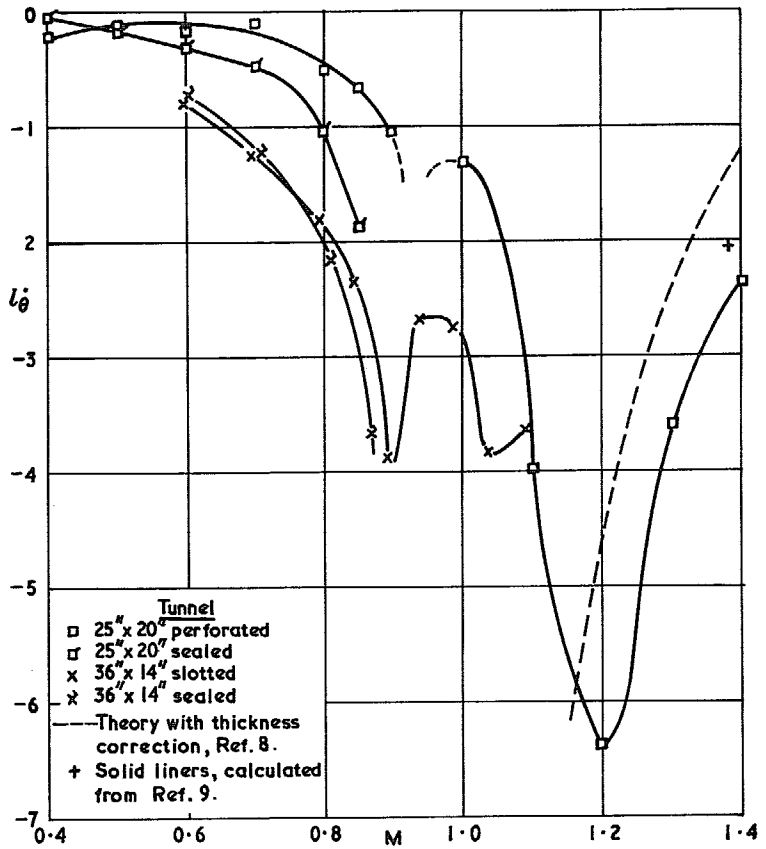

FIG. 17. Variation of derivative $l_{\dot{\theta}}$ with Mach number for tapered wing in two ventilated tunnels including supersonic speeds. $x_0 = 0{\cdot}79\bar{c}$.

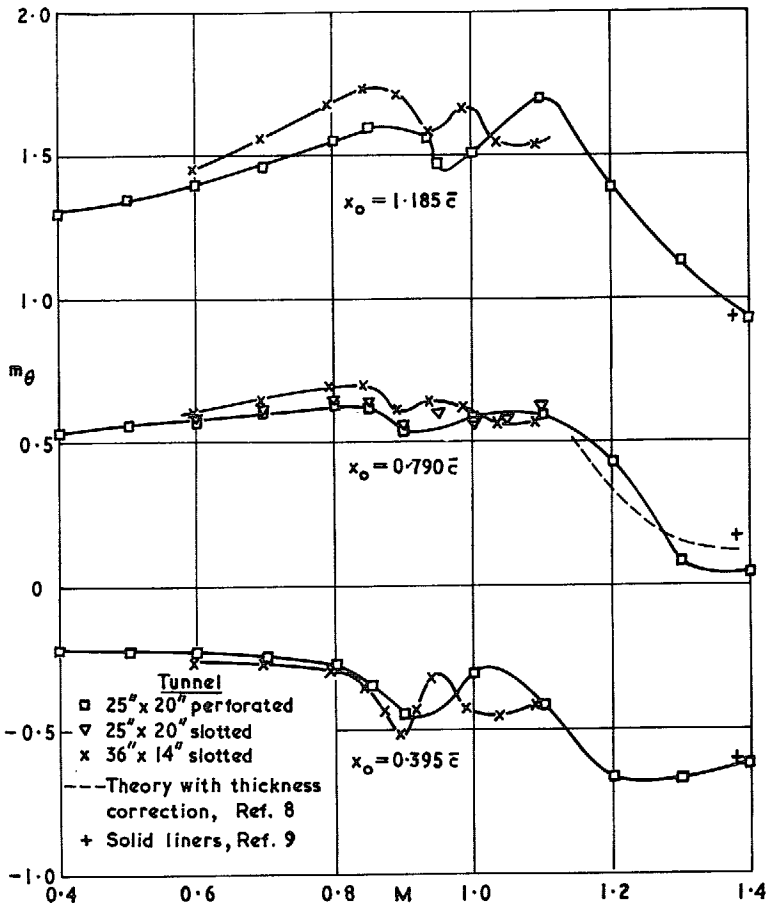

FIG. 18. Variation of derivative $m_{\dot{\theta}}$ with Mach number for tapered wing in two ventilated tunnels including supersonic speeds.

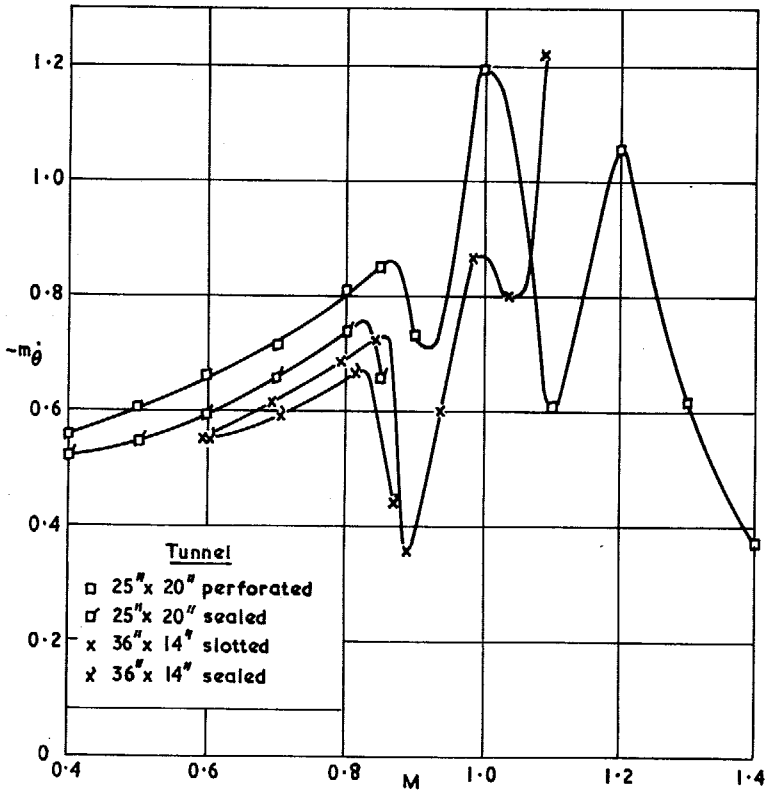

FIG. 19a. Variation of derivative $m_{\dot{\theta}}$ with Mach number for tapered wing in two ventilated tunnels including supersonic speeds. $x_0 = 0{\cdot}395\bar{c}$.

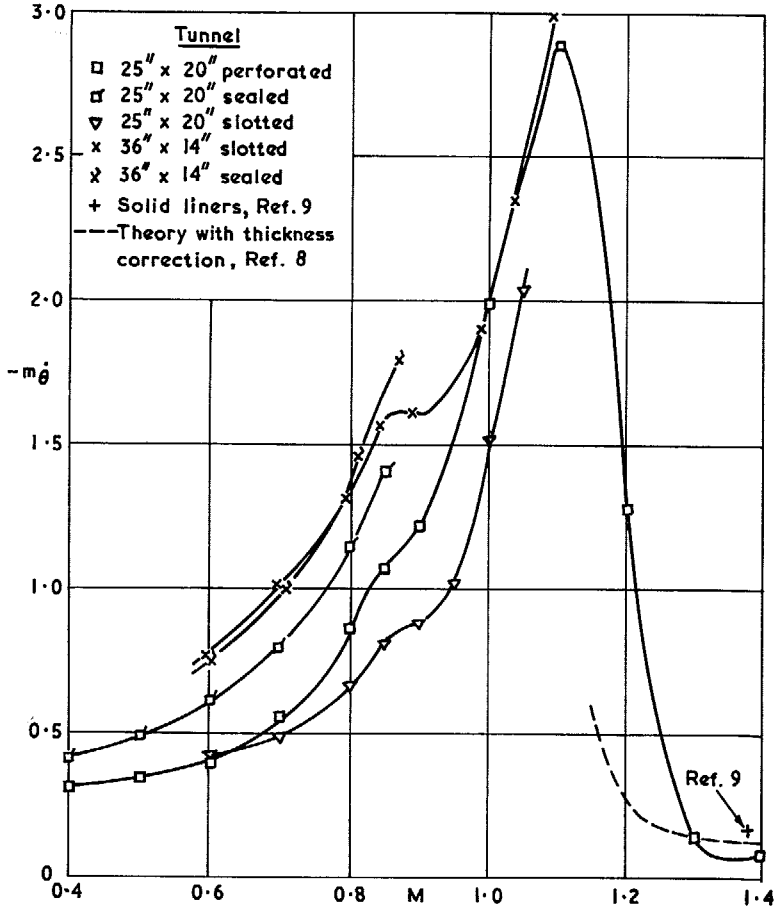

FIG. 19b. Variation of derivative $m_{\dot{\theta}}$ with Mach number for tapered wing in two ventilated tunnels including supersonic speeds. $x_0 = 0{\cdot}79\bar{c}$.

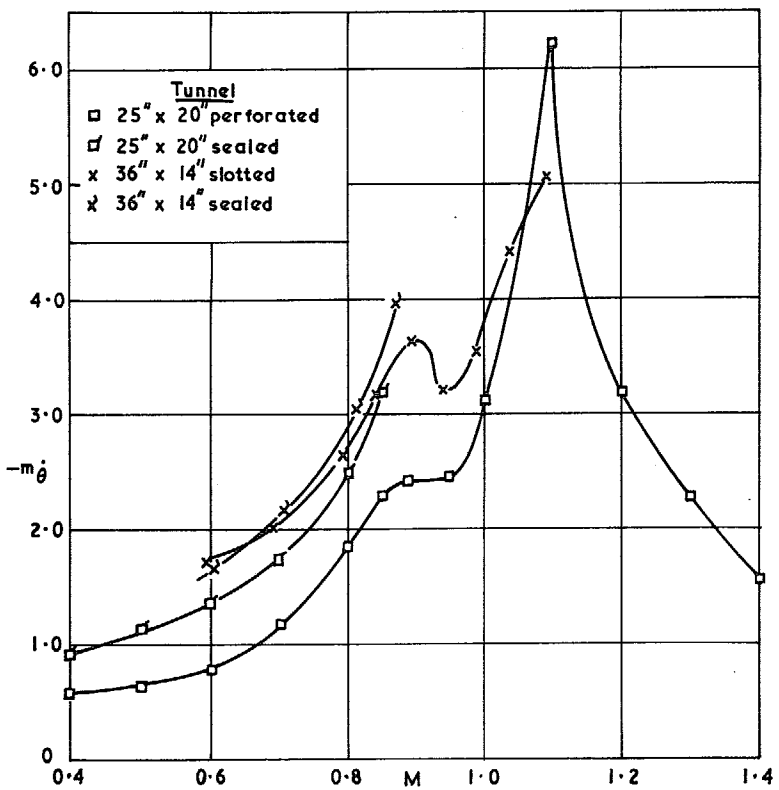

FIG. 19c. Variation of derivative $m_{\dot{\theta}}$ with Mach number for tapered wing in two ventilated tunnels including supersonic speeds. $x_0 = 1{\cdot}185\bar{c}$.

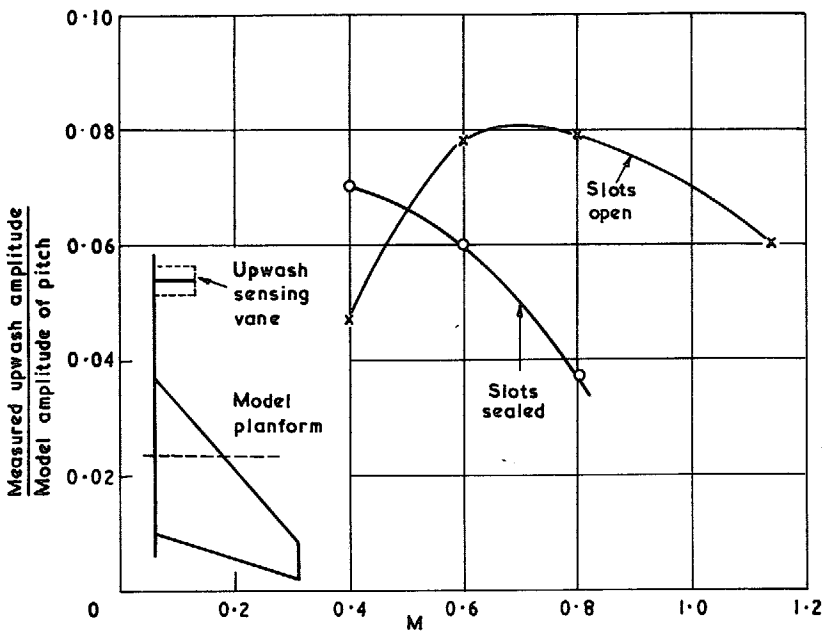

FIG. 20. Effect of Mach number on upwash measured at 1·04 root chords upstream of model pitching axis (Ref. 5).

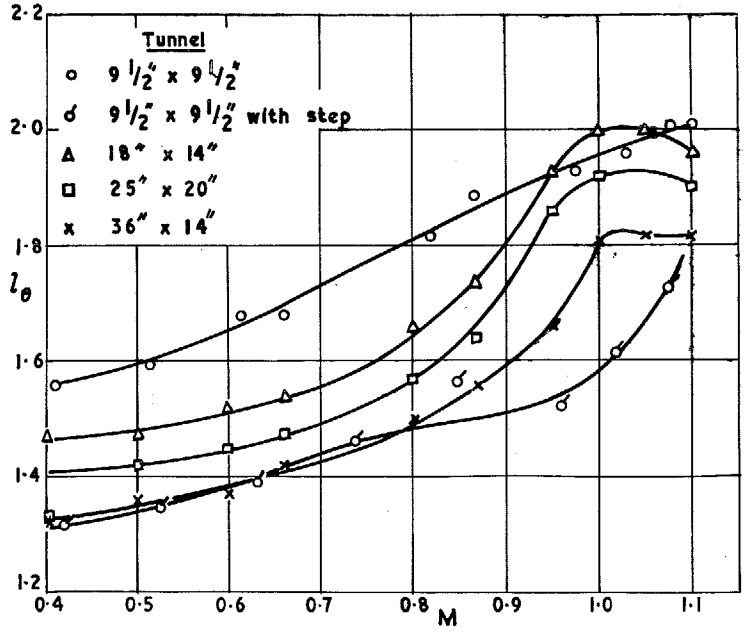

FIG .21. Corrected values of derivative l_θ for the delta wing in four ventilated tunnels including transonic speeds.

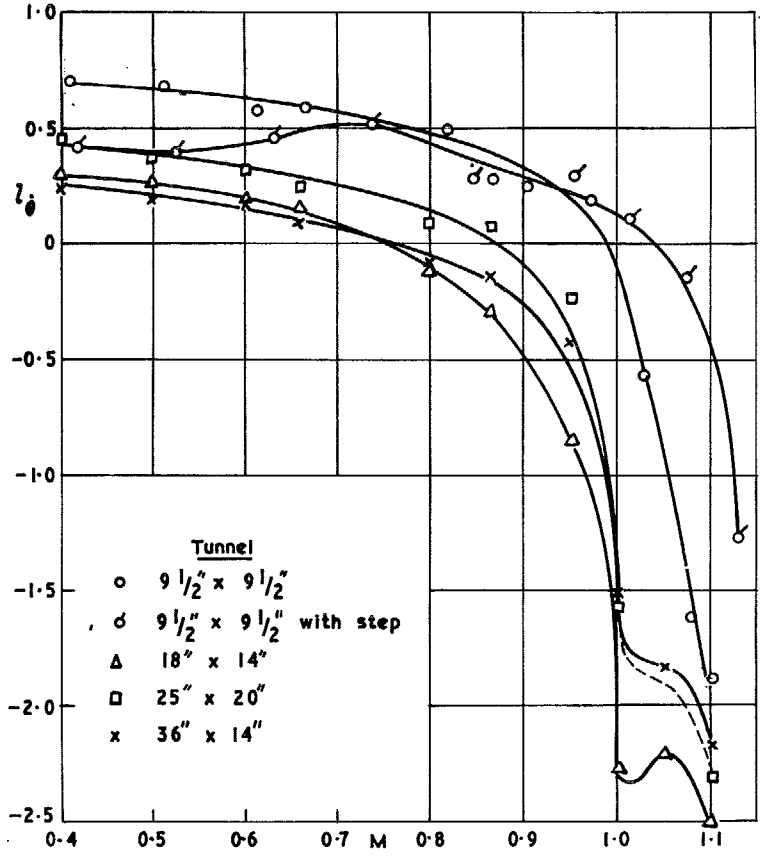

FIG. 22. Corrected values of derivative $l_{\dot\theta}$ for the delta wing in four ventilated tunnels including transonic speeds. $x_0 = 1{\cdot}04\bar{c}$.

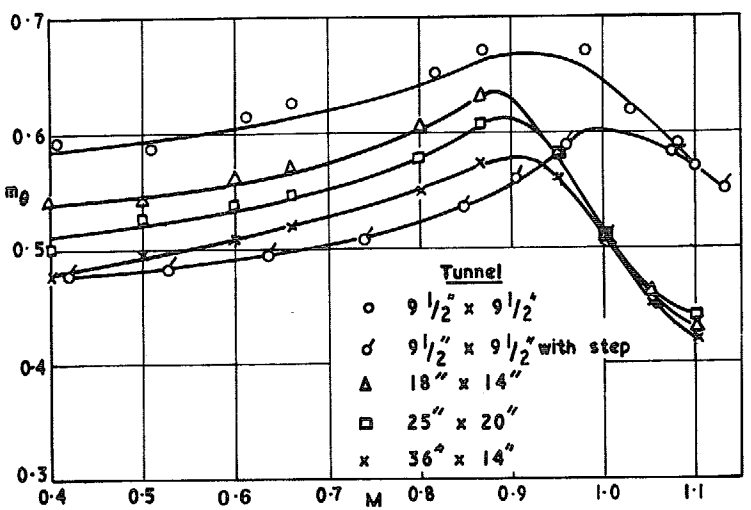

FIG. 23. Corrected values of derivative m_θ for the delta wing in four ventilated tunnels including transonic speeds. $x_0 = 1{\cdot}04\bar{c}$.

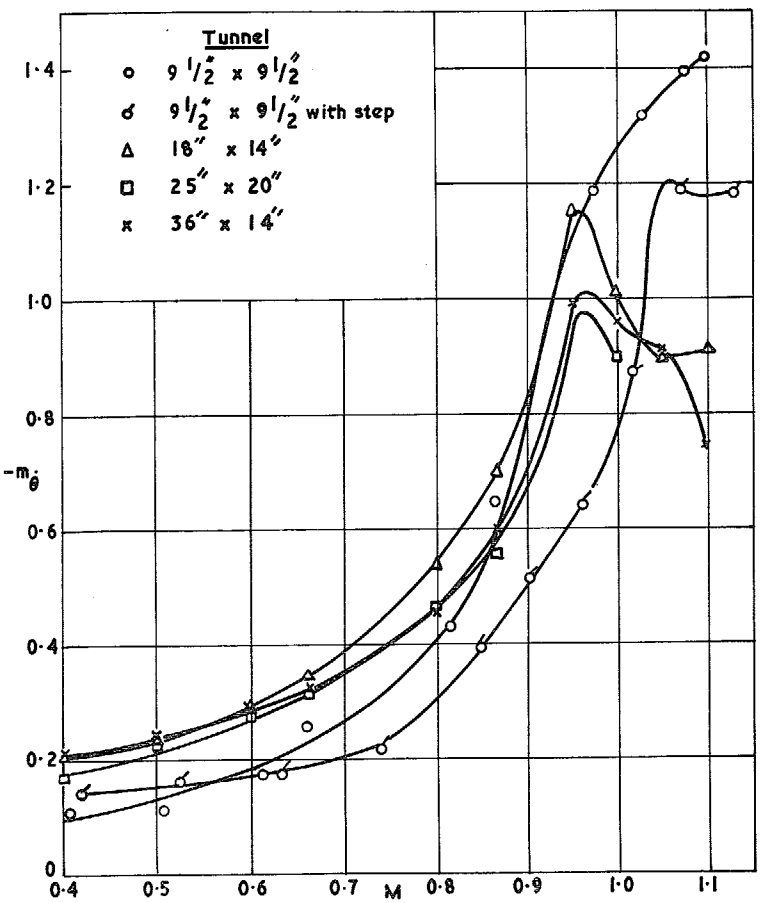

FIG. 24. Corrected values of derivative $m_{\dot\theta}$ for the delta wing in four ventilated tunnels including transonic speeds. $x_0 = 1{\cdot}04\bar{c}$.

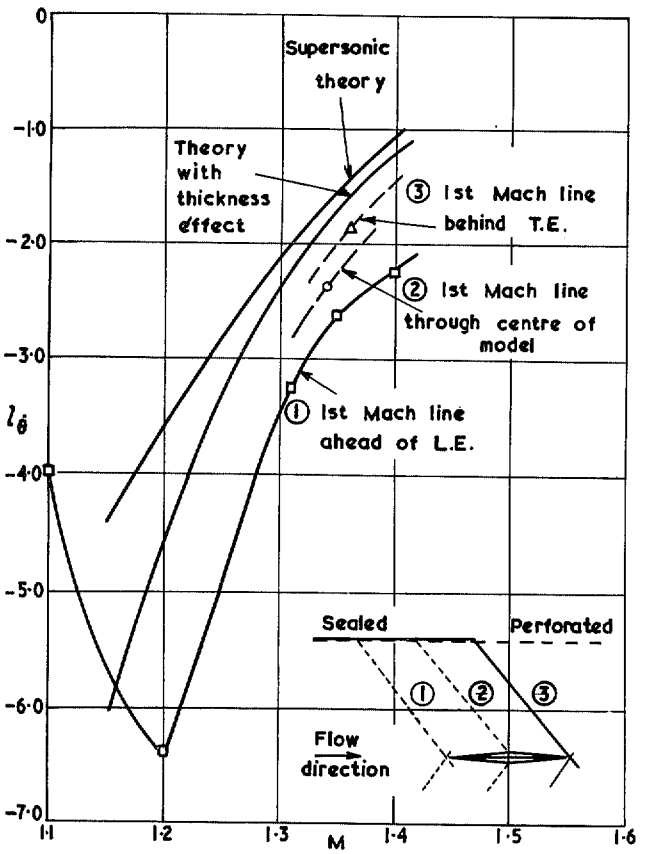

FIG. 25. Variation of $l_{\dot{\theta}}$ with Mach number at supersonic speeds for tapered wing in 25 in. × 20 in. tunnel. $x_0 = 0{\cdot}79\bar{c}$.

Printed in Wales for Her Majesty's Stationery Office by Allens Printers (Wales) Limited

Dd. 135646 K 5

Published by
HER MAJESTY'S STATIONERY OFFICE

To be purchased from
49 High Holborn, London W.C.1
13A Castle Street, Edinburgh 2
109 St. Mary Street, Cardiff CF1 1JW
Brazennose Street, Manchester M60 8AS
50 Fairfax Street, Bristol BS1 3DE
258 Broad Street, Birmingham 1
7 Linenhall Street, Belfast BT2 8AY
or through any bookseller

S.O. Code No. 23-357(